1 **Aqueous-phase mechanism for secondary organic aerosol formation from isoprene:**
2 **application to the Southeast United States and co-benefit of SO$_2$ emission controls**
3

4 E. A. Marais[1], D. J. Jacob[1,2], J. L. Jimenez[3,4], P. Campuzano-Jost[3,4], D. A. Day[3,4], W. Hu[3,4], J.
5 Krechmer[3,4], L. Zhu[1], P. S. Kim[2], C. C. Miller[2], J. A. Fisher[5], K. Travis[1], K. Yu[1], T. F. Hanisco[6],
6 G. M. Wolfe[6,7], H. L. Arkinson[8], H. O. T. Pye[9], K. D. Froyd[3,10], J. Liao[3,10], V. F. McNeill[11]
7

8 [1]School of Engineering and Applied Sciences, Harvard University, Cambridge, MA, USA.
9 [2]Earth and Planetary Sciences, Harvard University, Cambridge, MA, USA.
10 [3]Cooperative Institute for Research in Environmental Sciences, University of Colorado, Boulder, CO, USA.
11 [4]Department of Chemistry and Biochemistry, University of Colorado, Boulder, CO, USA.
12 [5]School of Chemistry and School of Earth and Environmental Sciences, University of Wollongong, Wollongong,
13 New South Wales, Australia.
14 [6]Atmospheric Chemistry and Dynamics Lab, NASA Goddard Space Flight Center, Greenbelt, MD, USA.
15 [7]Joint Center for Earth Systems Technology, University of Maryland Baltimore County, Baltimore, MD, USA.
16 [8]Department of Atmospheric and Oceanic Science, University of Maryland, College Park, MD, USA.
17 [9]National Exposure Research Laboratory, US EPA, Research Triangle Park, NC, USA.
18 [10]Chemical Sciences Division, Earth System Research Laboratory, NOAA, Boulder, Colorado, USA
19 [11]Department of Chemical Engineering, Columbia University, New York, New York 10027, USA.
20

21 **Abstract**

22   Isoprene emitted by vegetation is an important precursor of secondary organic aerosol
23 (SOA), but the mechanism and yields are uncertain. Aerosol is prevailingly aqueous under the
24 humid conditions typical of isoprene-emitting regions. Here we develop an aqueous-phase
25 mechanism for isoprene SOA formation coupled to a detailed gas-phase isoprene oxidation
26 scheme. The mechanism is based on aerosol reactive uptake coefficients (γ) for water-soluble
27 isoprene oxidation products, including sensitivity to aerosol acidity and nucleophile
28 concentrations. We apply this mechanism to simulation of aircraft (SEAC^{4}RS) and ground-based
29 (SOAS) observations over the Southeast US in summer 2013 using the GEOS-Chem chemical
30 transport model. Emissions of nitrogen oxides (NO$_x \equiv$ NO + NO$_2$) over the Southeast US are
31 such that the peroxy radicals produced from isoprene oxidation (ISOPO$_2$) react significantly with
32 both NO (high-NO$_x$ pathway) and HO$_2$ (low-NO$_x$ pathway), leading to different suites of
33 isoprene SOA precursors. We find a mean SOA mass yield of 3.3 % from isoprene oxidation,
34 consistent with the observed relationship of total fine organic aerosol (OA) and formaldehyde (a
35 product of isoprene oxidation). Isoprene SOA production is mainly contributed by two
36 immediate gas-phase precursors, isoprene epoxydiols (IEPOX, 58% of isoprene SOA) from the
37 low-NO$_x$ pathway and glyoxal (28%) from both low- and high-NO$_x$ pathways. This speciation is
38 consistent with observations of IEPOX SOA from SOAS and SEAC^{4}RS. Observations show a
39 strong relationship between IEPOX SOA and sulfate aerosol that we explain as due to the effect
40 of sulfate on aerosol acidity and volume. Isoprene SOA concentrations increase as NO$_x$
41 emissions decrease (favoring the low-NO$_x$ pathway for isoprene oxidation), but decrease more

42 strongly as SO_2 emissions decrease (due to the effect of sulfate on aerosol acidity and volume).

43 The US EPA projects 2013-2025 decreases in anthropogenic emissions of 34% for NO_x (leading

44 to 7% increase in isoprene SOA) and 48% for SO_2 (35% decrease in isoprene SOA). Reducing

45 SO_2 emissions decreases sulfate and isoprene SOA by a similar magnitude, representing a factor

46 of 2 co-benefit for $PM_{2.5}$ from SO_2 emission controls.

47

48 Keywords: isoprene, SOA yield, IEPOX, glyoxal, $SEAC^4RS$, SOAS, formaldehyde.

49

50 Corresponding Author: emarais@seas.harvard.edu

1. Introduction

Isoprene emitted by vegetation is a major source of secondary organic aerosol (SOA) (Carlton et al., 2009, and references therein) with effects on human health, visibility, and climate. There is large uncertainty in the yield and composition of isoprene SOA (Scott et al., 2014; McNeill et al., 2014), involving a cascade of species produced in the gas-phase oxidation of isoprene and their interaction with pre-existing aerosol (Hallquist et al., 2009). We develop here a new aqueous-phase mechanism for isoprene SOA formation coupled to gas-phase chemistry, implement it in the GEOS-Chem chemical transport model (CTM) to simulate observations in the Southeast US, and from there derive new constraints on isoprene SOA yields and the contributing pathways.

Organic aerosol is ubiquitous in the atmosphere, often dominating fine aerosol mass (Zhang et al., 2007), including in the Southeast US where it accounts for more than 60% in summer (Attwood et al., 2014). It may be directly emitted by combustion as primary organic aerosol (POA), or produced within the atmosphere as SOA by oxidation of volatile organic compounds (VOCs). Isoprene (C_5H_8) from vegetation is the dominant VOC emitted globally, and the Southeast US in summer is one of the largest isoprene-emitting regions in the world (Guenther et al., 2006). SOA yields from isoprene are low compared with larger VOCs (Pye et al., 2010), but isoprene emissions are much higher. Kim et al. (2015) estimated that isoprene accounts for 40% of total organic aerosol in the Southeast US in summer.

Formation of OA from oxidation of isoprene depends on local concentrations of nitrogen oxide radicals ($NO_x \equiv NO + NO_2$) and pre-existing aerosol. NO_x concentrations determine the fate of organic peroxy radicals originating from isoprene oxidation ($ISOPO_2$), leading to different cascades of oxidation products in the low-NO_x and high-NO_x pathways (Paulot et al.,

74   2009a; 2009b). Uptake of isoprene oxidation products to the aerosol phase depends on their

75   vapor pressure (Donahue et al., 2006), solubility in aqueous media (Saxena and Hildeman,

76   1996), and subsequent condensed-phase reactions (Volkamer et al., 2007). Aqueous aerosol

77   provides a medium for reactive uptake (Eddingsaas et al., 2010; Surratt et al., 2010) with

78   dependences on acidity (Surratt et al., 2007a), concentration of nucleophiles such as sulfate

79   (Surratt et al., 2007b), aerosol water (Carlton and Turpin, 2013), and organic coatings (Gaston et

80   al., 2014).

81   We compile in Fig. 1 the published laboratory yields of isoprene SOA as a function of

82   initial NO concentration and relative humidity (RH). Here and elsewhere, the isoprene SOA

83   yield is defined as the mass of SOA produced per unit mass of isoprene oxidized. Isoprene SOA

84   yields span a wide range, from <0.1% to >10%, with no systematic difference between low-NO_x

85   and high-NO_x pathways. Yields tend to be higher in dry chambers (RH < 10%). Under such dry

86   conditions isoprene SOA is expected to be solid (Virtanen et al., 2010; Song et al., 2015). At

87   humid conditions more representative of the summertime boundary layer, aerosols are likely

88   aqueous (Bateman et al., 2014). Standard isoprene SOA mechanisms used in atmospheric models

89   assume reversible partitioning onto pre-existing organic aerosol, fitting the dry chamber data

90   (Odum et al., 1996). However, this may not be appropriate for actual atmospheric conditions

91   where aqueous-phase chemistry with irreversible reactive uptake of water-soluble gases is likely

92   the dominant mechanism (Ervens et al., 2011; Carlton and Turpin, 2013). Several regional/global

93   models have implemented mechanisms for aqueous-phase formation of isoprene SOA (Fu et al.,

94   2008, 2009; Carlton et al., 2008; Myriokefalitakis et al., 2011; Liu et al., 2012; Pye et al., 2013;

95   Lin et al., 2014).

96   Here we present a mechanism for irreversible aqueous-phase isoprene SOA formation

97 integrated within a detailed chemical mechanism for isoprene gas-phase oxidation, thus linking

98 isoprene SOA formation to gas-phase chemistry and avoiding more generic volatility-based

99 parameterizations that assume dry organic aerosol (Odum et al., 1996; Donahue et al., 2006). We

100 use this mechanism in the GEOS-Chem CTM to simulate observations from the SOAS (surface)

101 and SEAC^{4}RS (aircraft) field campaigns over the Southeast US in summer 2013, with focus on

102 isoprene SOA components and on the relationship between OA and formaldehyde (HCHO).

103 HCHO is a high-yield oxidation product of isoprene (Palmer et al., 2003) and we use the OA-

104 HCHO relationship as a constraint on isoprene SOA yields. SOAS measurements were made at a

105 ground site in rural Centreville, Alabama (Hu et al., 2015; http://soas2013.rutgers.edu/).

106 SEAC^{4}RS measurements were made from the NASA DC-8 aircraft with extensive boundary

107 layer coverage across the Southeast (Toon et al., 2016; SEAC^{4}RS Archive).

108

109 **2. Chemical mechanism for isoprene SOA formation**

110   The default treatment of isoprene SOA in GEOS-Chem at the time of this work (v9-02;

111 http://geos-chem.org) followed a standard parameterization operating independently from the

112 gas-phase chemistry mechanism and based on reversible partitioning onto pre-existing OA of

113 generic semivolatile products of isoprene oxidation by OH and NO_3 radicals (Pye et al., 2010).

114 Here we implement a new mechanism for reactive uptake by aqueous aerosols of species

115 produced in the isoprene oxidation cascade of the GEOS-Chem gas-phase mechanism. This

116 couples SOA formation to the gas-phase chemistry and is in accord with increased evidence for a

117 major role of aqueous aerosols in isoprene SOA formation (Ervens et al., 2011).

118   The standard gas-phase isoprene oxidation mechanism in GEOS-Chem v9-02 is

119   described in Mao et al. (2013) and is based on best knowledge at the time building on

120   mechanisms for the oxidation of isoprene by OH (Paulot et al., 2009a; 2009b) and NO_3 (Rollins

121   et al., 2009). Updates implemented in this work are described below and in companion papers

122   applying GEOS-Chem to simulation of observed gas-phase isoprene oxidation products over the

123   Southeast US in summer 2013 (Fisher et al., 2016; Travis et al., 2016). Most gas-phase products

124   of the isoprene oxidation cascade in GEOS-Chem have high dry deposition velocity, competing

125   in some cases with removal by oxidation and aerosol formation (Nguyen et al., 2015a; Travis et

126   al., 2016).

127   Figure 2 shows the isoprene oxidation cascade in GEOS-Chem leading to SOA

128   formation. Reaction pathways leading to isoprene SOA precursors are described below. Yields

129   are in mass percent, unless stated otherwise. Reactive $ISOPO_2$ isomers formed in the first OH

130   oxidation step react with NO, the hydroperoxyl radical (HO_2), other peroxy radicals (RO_2), or

131   undergo isomerization (Peeters et al., 2009). The NO reaction pathway (high-NO_x pathway)

132   yields C_5 hydroxy carbonyls, methyl vinyl ketone, methacrolein, and first-generation isoprene

133   nitrates (ISOPN). The first three products go on to produce glyoxal and methylglyoxal, which

134   serve as SOA precursors. The overall yield of glyoxal from the high-NO_x pathway is 7 mol %

135   (yield on a molar basis). Oxidation of ISOPN by OH and O_3 is as described by Lee et al. (2014).

136   Reaction of ISOPN with OH produces saturated dihydroxy dinitrates (DHDN), 21 and 27 mol %

137   from the beta and delta channels respectively (Lee et al., 2014), and 10 mol % isoprene

138   epoxydiols (IEPOX) from each channel (Jacobs et al., 2014). We also adopt the mechanism of

139   Lin et al. (2013) to generate C_4 hydroxyepoxides (methacrylic acid epoxide and

140   hydroxymethylmethyl-α-lactone, both denoted MEPOX) from OH oxidation of a

141 peroxyacylnitrate formed when methacrolein reacts with OH followed by NO_2. Only

142 hydroxymethylmethyl-α-lactone is shown in Fig. 2.

143   The HO_2 reaction pathway for $ISOPO_2$ leads to formation of hydroxyhydroperoxides

144 (ISOPOOH) that are oxidized to IEPOX (Paulot et al., 2009b) and several low-volatility

145 products, represented here as C_5-LVOC (Krechmer et al., 2015). The kinetics of IEPOX

146 oxidation by OH is uncertain, and experimentally determined IEPOX lifetimes vary from 8 to 28

147 h for an OH concentration of 1×10^6 molecules cm^{-3} (Jacobs et al., 2013; Bates et al., 2014). In

148 GEOS-Chem we apply the fast kinetics of Jacobs et al. (2013) and reduce the yield of IEPOX

149 from ISOPOOH from 100 to 75%, within the range observed by St. Clair et al. (2016), to address

150 a factor of 4 overestimate in simulated IEPOX pointed out by Nguyen et al. (2015a). The IEPOX

151 discrepancy could alternatively be addressed with an order-of-magnitude increase in uptake by

152 aerosol (see below) but the model would then greatly overestimate the observed IEPOX SOA

153 concentrations in SOAS and SEAC^{4}RS (Section 4).

154   IEPOX oxidizes to form glyoxal and methylglyoxal (Bates et al., 2014). The overall

155 glyoxal yield from the $ISOPO_2 + HO_2$ pathway is 6 mol %. Krechmer et al. (2015) report a 2.5

156 mol % yield of C_5-LVOC from ISOPOOH but we reduce this to 0.5 mol % to reproduce surface

157 observations of the corresponding aerosol products (Section 4). Methyl vinyl ketone and

158 methacrolein yields from the $ISOPO_2 + HO_2$ pathway are 2.5 and 3.8 mol %, respectively (Liu et

159 al., 2013), sufficiently low that they do not lead to significant SOA formation.

160   Minor channels for $ISOPO_2$ are isomerization and reaction with RO_2. Isomerization

161 forms hydroperoxyaldehydes (HPALD) that go on to photolyze, but products are uncertain

162 (Peeters and Müller, 2010). We assume 25 mol % yield each of glyoxal and methylglyoxal from

163 HPALD photolysis in GEOS-Chem following Stavrakou et al. (2010). Reaction of $ISOPO_2$ with

164   RO_2 leads to the same suite of C_4-C_5 carbonyls as reaction with NO (C_5 hydroxy carbonyls,

165   methacrolein, and methyl vinyl ketone) and from there to glyoxal and methylglyoxal.

166   Immediate aerosol precursors from the isoprene + OH oxidation cascade are identified in

167   Fig. 2. For the high-NO_x pathway ($ISOPO_2$ + NO channel) these include glyoxal and

168   methylglyoxal (McNeill et al., 2012), ISOPN (Darer et al., 2011; Hu et al., 2011), DHDN (Lee et

169   al., 2014), MEPOX (Lin et al., 2013), and IEPOX (Jacobs et al., 2014). For the low-NO_x

170   pathway ($ISOPO_2$ + HO_2 channel) aerosol precursors are IEPOX (Eddingsaas et al., 2010), C_5-

171   LVOC (Krechmer et al., 2015, in which the aerosol-phase species is denoted ISOPOOH-SOA),

172   glyoxal, and methylglyoxal. Glyoxal and methylglyoxal are also produced from the $ISOPO_2$ +

173   RO_2 and $ISOPO_2$ isomerization channels.

174   Ozonolysis and oxidation by NO_3 are additional minor isoprene reaction pathways (Fig.

175   2). The NO_3 oxidation pathway is a potentially important source of isoprene SOA at night

176   (Brown et al., 2009) from the irreversible uptake of low-volatility second-generation

177   hydroxynitrates (NT-ISOPN) (Ng et al., 2008; Rollins et al., 2009). We update the gas-phase

178   chemistry of Rollins et al. (2009) as implemented by Mao et al. (2013) to include formation of 4

179   mol % of the aerosol-phase precursor NT-ISOPN from first-generation alkylnitrates (Rollins et

180   al., 2009). Ozonolysis products are volatile and observed SOA yields in chamber studies are low

181   (< 1%; Kleindienst et al., 2007). In GEOS-Chem only methylglyoxal is an aerosol precursor

182   from isoprene ozonolysis.

183   We implement uptake of isoprene oxidation products to aqueous aerosols using

184   laboratory-derived reactive uptake coefficients (γ) as given by Anttila et al. (2006) and Gaston et

185   al. (2014):

186

187 $$\gamma = \left[\frac{1}{\alpha} + \frac{3\omega}{4rRTH^*k_{aq}} \right]^{-1}$$ (1).

188

189 Here α is the mass accommodation coefficient (taken as 0.1 for all immediate SOA precursors in

190 Fig. 2), ω is the mean gas-phase molecular speed (cm s^{-1}), r is the aqueous particle radius (cm), R

191 is the universal gas constant (0.08206 L atm K^{-1} mol^{-1}), T is temperature (K), H^* is the effective

192 Henry's Law constant (M atm^{-1}) accounting for any fast dissociation equilibria in the aqueous

193 phase, and k_{aq} is the pseudo first-order aqueous-phase reaction rate constant (s^{-1}) for conversion

194 to non-volatile products.

195   Precursors with epoxide functionality, IEPOX and MEPOX, undergo acid-catalyzed

196 epoxide ring opening and nucleophilic addition in the aqueous phase. The aqueous-phase rate

197 constant formulation is from Eddingsaas et al. (2010),

198

199 $$k_{aq} = k_{H^+}\left[H^+ \right] + k_{nuc}\left[nuc \right]\left[H^+ \right] + k_{HSO_4^-}\left[HSO_4^- \right]$$ (2),

200

201 and includes three channels: acid-catalyzed ring opening followed by nucleophilic addition of

202 H$_2$O (k_{H^+} in M^{-1} s^{-1}) leading to methyltetrols, acid-catalyzed ring opening followed by

203 nucleophilic addition of sulfate and nitrate ions ($nuc \equiv SO_4^{2-} + NO_3^-$, k_{nuc} in M^{-2} s^{-1}) leading to

204 organosulfates and organonitrates, and concerted protonation and nucleophilic addition by

205 bisulfate, HSO$_4^-$ (k_{HSO4-} in M^{-1} s^{-1}), leading to organosulfates.

206   Precursors with nitrate functionality (-ONO$_2$), ISOPN and DHDN, hydrolyze to form

207 low-volatility polyols and nitric acid (Hu et al., 2011; Jacobs et al., 2014), so k_{aq} in Eq. (1) is the

208 hydrolysis rate constant.

209   Glyoxal and methylglyoxal form SOA irreversibly by surface uptake followed by

210   aqueous-phase oxidation and oligomerization to yield non-volatile products (Liggio et al., 2005;

211   Volkamer et al., 2009; Nozière et al., 2009; Ervens et al., 2011; Knote et al., 2014). Glyoxal

212   forms SOA with higher yields during the day than at night due to OH aqueous-phase chemistry

213   (Tan et al., 2009; Volkamer et al., 2009; Summer et al., 2014). We use a daytime γ of 2.9×10^{-3}

214   for glyoxal from Liggio et al. (2005) and a nighttime γ of 5×10^{-6} (Waxman et al., 2013; Sumner

215   et al., 2014). The SOA yield of methylglyoxal is small compared with that of glyoxal (McNeill et

216   al., 2012). A previous GEOS-Chem study by Fu et al. (2008) used the same γ (2.9×10^{-3}) for

217   glyoxal and methylglyoxal. Reaction rate constants are similar for aqueous-phase processing of

218   glyoxal and methylglyoxal (Buxton et al., 1997; Ervens et al., 2003), but H^* of glyoxal is about 4

219   orders of magnitude higher. Here we scale the γ for methylglyoxal to the ratio of effective

220   Henry's law constants: $H^* = 3.7 \times 10^3$ M atm^{-1} for methylglyoxal (Tan et al., 2010) and $H^* = 2.7$

221   $\times 10^7$ M atm^{-1} for glyoxal (Sumner et al., 2014). The resulting uptake of methylglyoxal is very

222   slow and makes a negligible contribution to isoprene SOA.

223   The species C_5-LVOC from ISOPOOH oxidation and NT-ISOPN from isoprene reaction

224   with NO_3 have very low volatility and are assumed to condense to aerosols with a γ of 0.1

225   limited by mass accommodation. Results are insensitive to the precise value of γ since uptake by

226   aerosols is the main sink for these species in any case.

227   Table 1 gives input variables used to calculate γ for IEPOX, ISOPN, and DHDN by Eqs.

228   (1) and (2). Rate constants are from experiments in concentrated media, representative of

229   aqueous aerosols, so no activity correction factors are applied. Reported experimental values of

230   k_{H+} vary by an order of magnitude from 1.2×10^{-3} M^{-1} s^{-1} (Eddingsaas et al., 2010) to 3.6×10^{-2}

231   M^{-1} s^{-1} (Cole-Filipiak et al., 2010). Values of k_{nuc} vary by 3 orders of magnitude from 2×10^{-4} M^{-}

232   ^{2} s^{-1} (Eddingsaas et al., 2010) to 5.2×10^{-1} M^{-2} s^{-1} (Piletic et al., 2013). Reported values of

233   IEPOX H^* vary by two orders of magnitude (Eddingsaas et al., 2010; Nguyen et al., 2014). We

234   chose values of k_{H+}, k_{nuc}, and H^* to fit the SOAS and SEAC^{4}RS observations of total IEPOX

235   SOA and IEPOX organosulfates, as discussed in Section 4.

236   Table 2 lists average values of γ for all immediate aerosol precursors in the Southeast US

237   boundary layer in summer as simulated by GEOS-Chem (Section 3). γ for IEPOX is a strong

238   function of pH and increases from 1×10^{-4} to 1×10^{-2} as pH decreases from 3 to 0. Gaston et al.

239   (2014) reported order-of-magnitude higher values of γ for IEPOX, reflecting their use of a higher

240   H^*, but this would lead in our model to an overestimate of IEPOX SOA observations (Section 4).

241   The value of γ for MEPOX is assumed to be 30 times lower than that of IEPOX when the aerosol

242   is acidic (pH < 4), due to slower acid-catalyzed ring opening (Piletic et al., 2013; Riedel et al.,

243   2015). At pH > 4 we assume that γ for IEPOX and MEPOX are the same (Riedel et al., 2015),

244   but they are then very low.

245   Isoprene SOA formation in clouds is not considered here. Acid-catalyzed pathways

246   would be slow. Observations show that the isoprene SOA yield in the presence of laboratory-

247   generated clouds is low (0.2-0.4%; Brégonzio-Rozier et al., 2015). Wagner et al. (2015) found no

248   significant production of SOA in boundary layer clouds over the Southeast US during SEAC^{4}RS.

249

250   **3. GEOS-Chem simulation and isoprene SOA yields**

251   Several companion papers apply GEOS-Chem to interpret SEAC^{4}RS and surface data

252   over the Southeast US in summer 2013 including Kim et al. (2015) for aerosols, Fisher et al.

253   (2016) for organic nitrates, Travis et al. (2016) for ozone and NO$_x$, and Zhu et al. (2016) for

254   HCHO. These studies use a model version with 0.25° × 0.3125° horizontal resolution over North

255 America, nested within a 4° × 5° global simulation. Here we use a 2° × 2.5° global GEOS-Chem

256 simulation with no nesting. Yu et al. (2016) found little difference between 0.25° × 0.3125° and

257 2° × 2.5° resolutions in simulated regional statistics for isoprene chemistry.

258   The reader is referred to Kim et al. (2015) for a general presentation of the model, the

259 treatment of aerosol sources and sinks, and evaluation with Southeast US aerosol observations;

260 and to Travis et al. (2016) and Fisher et al. (2016) for presentation of gas-phase chemistry and

261 comparisons with observed gas-phase isoprene oxidation products. Isoprene emission is from the

262 MEGAN v2.1 inventory (Guenther et al., 2012). The companion papers decrease isoprene

263 emission by 15% from the MEGAN v2.1 values to fit the HCHO data (Zhu et al., 2016), but this

264 is not applied here.

265   Our SOA simulation differs from that of Kim et al. (2015). They assumed fixed 3% and

266 10% mass yields of SOA from isoprene and monoterpenes, respectively, and parameterized SOA

267 formation from anthropogenic and open fire sources as a kinetic irreversible process following

268 Hodzic and Jimenez (2011). Here we use our new aqueous-phase mechanism for isoprene SOA

269 coupled to gas-phase chemistry as described in Section 2, and otherwise use the semivolatile

270 reversible partitioning scheme of Pye et al. (2010) for monoterpene, anthropogenic, and open fire

271 SOA. Kim et al. (2015) found no systematic bias in detailed comparisons to OA measurements

272 from SEAC[4]RS and from surface networks. We find a low bias, as shown below, because the

273 reversible partitioning scheme yields low anthropogenic and open fire SOA concentrations.

274   Organic aerosol and sulfate contribute most of the aerosol mass over the Southeast US in

275 summer, while nitrate is negligibly small (Kim et al., 2015). GEOS-Chem uses the ISORROPIA

276 thermodynamic model (Fountoukis and Nenes, 2007) to simulate sulfate-nitrate-ammonium

277 (SNA) aerosol composition, water content, and acidity as a function of local conditions.

278 Simulated aerosol pH along the SEAC[4]RS flight tracks in the Southeast US boundary layer

279 averages 1.3 (interquartiles 0.92 and 1.8). The aerosol pH remains below 3 even when sulfate

280 aerosol is fully neutralized by ammonia (Guo et al., 2015).

281　　　We consider that the aqueous aerosol population where isoprene SOA formation can take

282 place is defined by the sulfate aerosol population. This assumes that all aqueous aerosol particles

283 contain some sulfate, and that all sulfate is aqueous. Clear-sky RH measured from the aircraft in

284 the Southeast US boundary layer during SEAC[4]RS averaged 72 ± 17%, and the corresponding

285 values in GEOS-Chem sampled along the flight tracks averaged 66 ± 16%). These RHs are

286 sufficiently high that sulfate aerosol can reliably be expected to be aqueous (Wang et al., 2008).

287 The rate of gas uptake by the sulfate aerosol is computed with the pseudo-first order reaction rate

288 constant k_{het} (s[-1]) (Schwartz, 1986; Jacob, 2000):

289

290 $$k_{het} = \int_0^\infty 4\pi r^2 \left(\frac{r}{D_g} + \frac{4}{\gamma\omega} \right)^{-1} n(r)dr \qquad (3),$$

291

292 where D_g is the gas-phase diffusion constant (taken to be 0.1 cm^2 s^{-1}) and $n(r)$ is the number size

293 distribution of sulfate aerosol (cm^{-4}). The first and second terms in parentheses describe the

294 limitations to gas uptake from gas-phase diffusion and aqueous-phase reaction, respectively.

295　　　The sulfate aerosol size distribution including RH-dependent hygroscopic growth factors

296 is from the Global Aerosol Data Set (GADS) of Koepke et al. (1997), as originally implemented

297 in GEOS-Chem by Martin et al. (2003) and updated by Drury et al. (2010). The GADS size

298 distribution compares well with observations over the eastern US in summer (Drury et al., 2010),

299 including for SEAC[4]RS (Kim et al., 2015). We compute $n(r)$ locally in GEOS-Chem by taking

300   the dry SNA mass concentration, converting from mass to volume with a dry aerosol mass

301   density of 1700 kg m^{-3} (Hess et al., 1998), applying the aerosol volume to the dry sulfate size

302   distribution in GADS, and then applying the GADS hygroscopic growth factors. We verified that

303   the hygroscopic growth factors from GADS agree within 10% with those computed locally from

304   ISORROPIA.

305   Figure 2 shows the mean branching ratios for isoprene oxidation in the Southeast US

306   boundary layer as calculated by GEOS-Chem. 87% of isoprene reacts with OH, 8% with ozone,

307   and 5% with NO_3. Oxidation of isoprene by OH produces $ISOPO_2$ of which 51% reacts with NO

308   (high-NO_x pathway), 35% reacts with HO_2, 8% isomerizes, and 6% reacts with other RO_2

309   radicals.

310   Glyoxal is an aerosol precursor common to all isoprene + OH pathways in our

311   mechanism with yields of 7 mol % from the $ISOPO_2$ + NO pathway, 6 mol % from $ISOPO_2$ +

312   HO_2, 11 mol % from $ISOPO_2$ + RO_2, and 25 mol % from $ISOPO_2$ isomerization. For the

313   Southeast US conditions we thus find that 44% of glyoxal is from the $ISOPO_2$ + NO pathway,

314   24% from $ISOPO_2$ + HO_2, 8% from $ISOPO_2$ + RO_2, and 24% from $ISOPO_2$ isomerization.

315   The mean total yield of isoprene SOA computed in GEOS-Chem for the Southeast US

316   boundary layer is 3.3%, as shown in Fig. 2. IEPOX contributes 1.9% and glyoxal 0.9%. The low-

317   NO_x pathway involving $ISOPO_2$ reaction with HO_2 contributes 73% of the total isoprene SOA

318   yield, mostly from IEPOX, even though this pathway is only 35% of the fate of $ISOPO_2$. The

319   high-NO_x pathway contributes 16% of isoprene SOA, mostly from glyoxal. MEPOX

320   contribution to isoprene SOA is small (2%) and consistent with a recent laboratory study that

321   finds low SOA yields from this pathway under humid conditions (Nguyen et al., 2015b). The

322   minor low-NO_x pathways from $ISOPO_2$ isomerization and reaction with RO_2 contribute 8% of

14

323 isoprene SOA through glyoxal. The remainder of isoprene SOA formation (3%) is from

324 nighttime oxidation by NO_3.

325   The dominance of IEPOX and glyoxal as precursors for isoprene SOA was previously

326 found by McNeill et al. (2012) using a photochemical box model. Both IEPOX and glyoxal are

327 produced photochemically, and both are removed photochemically in the gas phase by reaction

328 with OH (and photolysis for glyoxal). The mean lifetimes of IEPOX and glyoxal against gas-

329 phase photochemical loss average 1.6 and 2.3 h respectively for SEAC[4]RS daytime conditions;

330 mean lifetimes against reactive uptake by aerosol are 31 and 20 hours, respectively. For both

331 species, aerosol uptake is thus a minor sink competing with gas-phase photochemical loss.

332 Although we have assumed here the fast gas-phase kinetics from Jacobs et al. (2013) for the

333 IEPOX + OH reaction, this result would not change if we used the slower kinetics from Bates et

334 al. (2014).

335   The dominance of gas-phase loss over aerosol uptake for both IEPOX and glyoxal

336 implies that isoprene SOA formation is highly sensitive to their reactive uptake coefficients γ and

337 to the aqueous aerosol mass concentration (in both cases, γ is small enough that uptake is

338 controlled by bulk aqueous-phase rather than surface reactions). We find under SEAC[4]RS

339 conditions that γ for IEPOX is mainly controlled by the H^+ concentration ($k_{H+}[H^+]$ in Eq. (2)),

340 with little contribution from nucleophile-driven and HSO_4^--driven channels, although this is

341 based on highly uncertain rate constants (Section 2). Consistency with SOAS and SEAC[4]RS

342 observations will be discussed below.

343   The 3.3% mean yield of isoprene SOA from our mechanism is consistent with the fixed

344 yield of 3% assumed by Kim et al. (2015) in their GEOS-Chem simulation of the SEAC[4]RS

345 period, including extensive comparisons to OA observations that showed a 40% mean

15

346   contribution of isoprene to total OA. We conducted a sensitivity simulation using the default

347   isoprene SOA mechanism in GEOS-Chem based on reversible partitioning of semivolatile

348   oxidation products onto pre-existing OA (Pye et al., 2010). The isoprene SOA yield in that

349   simulation was only 1.1%. The observed correlation of OA with HCHO in SEAC[4]RS supports

350   our higher yield, as shown below.

351

4. Observational constraints on isoprene SOA yields

353   Isoprene is the largest source of HCHO in the Southeast US (Millet et al., 2006), and we

354   use the observed relationship between OA and HCHO to evaluate the GEOS-Chem isoprene

355   SOA yields. The SEAC[4]RS aircraft payload included measurements of OA from an Aerodyne

356   Aerosol Mass Spectrometer (HR-ToF-AMS; DeCarlo et al, 2006; Canagaratna et al, 2007)

357   concurrent with HCHO from a laser-induced fluorescence instrument (ISAF; Cazorla et al.,

358   2015). Column HCHO was also measured during SEAC[4]RS from the OMI satellite instrument

359   (González Abad et al., 2015; Zhu et al., 2016), providing a proxy for isoprene emission (Palmer

360   et al., 2003; 2006).

361   Figure 3 (left) shows the observed and simulated relationships between OA and HCHO

362   mixing ratios in the boundary layer. There is a strong correlation in the observations and in the

363   model ($R = 0.79$ and $R = 0.82$, respectively). OA simulated with our aqueous-phase isoprene

364   SOA mechanism reproduces the observed slope (2.8 ± 0.3 μg sm^{-3} $ppbv^{-1}$, vs. 3.0 ± 0.4 μg sm^{-3}

365     $ppbv^{-1}$ in the observations). Similarly strong correlations and consistency between model and

366   observations are found with column HCHO measured from OMI (Fig. 3, right). The estimated

367   error on individual OMI HCHO observations is about 30% (Millet et al., 2006).

368   Also shown in Fig. 3 is a sensitivity simulation with the default GEOS-Chem mechanism

369   based on reversible partitioning with pre-existing organic aerosol (Pye et al., 2010) and

370   producing a 1.1% mean isoprene SOA yield, as compared to 3.3% in our simulation with the

371   aqueous-phase mechanism. That sensitivity simulation shows the same OA-HCHO correlation

372   (R = 0.82) but underestimates the slope (2.0 ± 0.3 µg sm^{-3} ppbv^{-1}). The factor of 3 increase in our

373   isoprene SOA yield does not induce a proportional increase in the slope, as isoprene contributes

374   only ~ 40% of OA in the Southeast US. But the slope is sensitive to the isoprene SOA yield, and

375   the good agreement between our simulation and observations supports our estimate of a mean

376   3.3% yield for the Southeast US.

377   Figure 3 shows an offset between the model and observations illustrated by the regression

378   lines. We overestimate HCHO by 0.4 ppbv on average because we did not apply the 15%

379   downward correction to MEGAN v2.1 isoprene emissions (Zhu et al., 2016). We also

380   underestimate total OA measured by the AMS in the boundary layer by 1.1 µg sm^{-3} (mean AMS

381   OA is 5.8 ± 4.3 µg sm^{-3}; model OA is 4.7 ± 4.4 µg sm^{-3}). The bias can be explained by our

382   omission of anthropogenic and open fire SOA, found by Kim et al. (2015) to account on average

383   for 18% of OA in SEAC^{4}RS.

384   Figure 4 shows time series of the isoprene SOA components IEPOX SOA and C$_5$-LVOC

385   SOA at Centreville, Alabama during SOAS. AMS observations from Hu et al. (2015) and

386   Krechmer et al. (2015) are compared to model values. IEPOX SOA and C$_5$-LVOC SOA are on

387   average 17% and 2% of total AMS OA, respectively (Hu et al., 2015; Krechmer et al., 2015).

388   The model reproduces mean IEPOX SOA and C$_5$-LVOC SOA without bias, supporting the

389   conclusion that IEPOX is the dominant contributor to isoprene SOA in the Southeast US (Fig. 2).

17

390   Figure 5 shows the relationships of daily mean IEPOX SOA and sulfate concentrations at

391   Centreville and in the SEAC[4]RS boundary layer. The same factor analysis method was used to

392   derive IEPOX SOA in SEAC[4]RS as in SOAS, however the uncertainty is larger for the aircraft

393   observations due to the much wider range of conditions encountered. There is a strong

394   correlation between IEPOX SOA and sulfate, both in observations and the model, with similar

395   slopes. Correlation between IEPOX SOA and sulfate has similarly been observed at numerous

396   Southeast US monitoring sites (Budisulistiorini et al., 2013; 2015; Xu et al., 2015; Hu et al.,

397   2015). Xu et al. (2015) concluded that IEPOX SOA may form by nucleophilic addition of sulfate

398   (sulfate channels in Eq. (2)) leading to organosulfates. However, we find in our model that the

399   H^+-catalyzed channel ($k_{H+}[H^+]$ term in Eq. (2)) contributes 90% of IEPOX SOA formation

400   throughout the Southeast US boundary layer, and that sulfate channels play only a minor role.

401   The correlation of IEPOX SOA and sulfate in the model is because increasing sulfate drives an

402   increase in aqueous aerosol volume and acidity. Although dominance of the H^+-catalyzed

403   channel is sensitive to uncertainties in the rate constants (Section 2), measurements from the

404   PALMS laser mass spectrometer during SEAC[4]RS (Liao et al., 2015) show a mean IEPOX

405   organosulfate concentration of 0.13 μg sm^{-3}, amounting to at most 9% of total IEPOX SOA. The

406   organosulfate should be a marker of the sulfate channels because its hydrolysis is negligibly slow

407   (Hu et al., 2011).

408   Correlation between IEPOX SOA and sulfate is also apparent in the spatial distribution of

409   IEPOX SOA, as observed by the SEAC[4]RS aircraft below 2 km and simulated by GEOS-Chem

410   along the aircraft flight tracks (Fig. 6). The correlation between simulated and observed IEPOX

411   SOA in Fig. 6 is R = 0.70. Average (mean) IEPOX SOA is 1.4 ± 1.4 μg sm^{-3} in the observations

412   and 1.3 ± 1.2 μg sm^{-3} in the model. The correlation between IEPOX SOA and sulfate is 0.66 in

413   the observations and 0.77 in the model. IEPOX SOA concentrations are highest in the industrial

414   Midwest and Kentucky, and in Louisiana-Mississippi, coincident with the highest sulfate

415   concentrations sampled on the flights. We also see in Fig. 6 frequent observations of very low

416   IEPOX SOA (less than 0.4 μg sm^{-3}) that are well captured by the model. These are associated

417   with very low sulfate (less than 1 μg sm^{-3}).

418   The mean IEPOX SOA concentration simulated by the model for the SEAC^{4}RS period

419   (background contours in Fig. 6) is far more uniform than IEPOX SOA simulated along the flight

420   tracks. This shows the importance of day-to-day variations in sulfate in driving IEPOX SOA

421   variability. IEPOX SOA contributed on average 24% of total OA in the SEAC^{4}RS observations,

422   and 28% in GEOS-Chem sampled along the flight tracks and as a regional mean. With IEPOX

423   SOA accounting for 58% of isoprene SOA in the model (Fig. 2), this amounts to a 41-48%

424   contribution of isoprene to total OA, consistent with the previous estimate of 40% by Kim et al.

425   (2015).

426

427   **5. Effect of Anthropogenic Emission Reductions**

428   The EPA projects that US anthropogenic emissions of NO$_x$ and SO$_2$ will decrease

429   respectively by 34% and 48% from 2013 to 2025 (EPA, 2014). We conducted a GEOS-Chem

430   sensitivity simulation to examine the effect of these changes on isoprene SOA, assuming no

431   other changes and further assuming that the emission decreases are uniform across the US.

432   Figure 7 shows the individual and combined effects of NO$_x$ and SO$_2$ emission reductions

433   on the branching pathways for isoprene oxidation, sulfate mass concentration, aerosol pH, and

434   isoprene SOA in the Southeast US boundary layer in summer. Reducing NO$_x$ emission by 34%

435   decreases the mean NO concentration by only 23%, in part because decreasing OH increases the

436   NO_x lifetime and in part because decreasing ozone increases the NO/NO_2 ratio. There is no

437   change in HO_2. We find a 10% decrease in the high-NO_x pathway and a 6% increase in the low-

438   NO_x pathway involving $ISOPO_2 + HO_2$. Aerosol sulfate decreases by 2% and there is no change

439   in $[H^+]$. The net effect is a 7% increase in isoprene SOA, as the major individual components

440   IEPOX SOA and glyoxal SOA increase by 17% and decrease by 8%, respectively.

441   A 48% decrease in SO_2 emissions drives a 36% reduction in sulfate mass concentration,

442   leading to a decline in aerosol volume (31%) that reduces uptake of all isoprene SOA precursors.

443   The decrease in aerosol $[H^+]$ (26%) further reduces IEPOX uptake. Decline in aerosol volume

444   and $[H^+]$ have a comparable effect on IEPOX SOA, as the change in each due to SO_2 emission

445   reductions is similar (~30%) and uptake of IEPOX SOA is proportional to the product of the two

446   (Section 4). IEPOX SOA and glyoxal SOA decrease by 45% and 26%, respectively, and total

447   isoprene SOA decreases by 35%. Pye et al. (2013) included uptake of IEPOX to aqueous

448   aerosols in a regional chemical transport model and similarly found that SO_2 emissions are more

449   effective than NO_x emissions at reducing IEPOX SOA in the Southeast US. Remarkably, we find

450   that reducing SO_2 emissions decreases sulfate and isoprene SOA with similar effectiveness (Fig.

451   7). With sulfate contributing ~30% of present-day $PM_{2.5}$ in the Southeast US and isoprene SOA

452   contributing ~25% (Kim et al., 2015), this represents a factor of 2 co-benefit on $PM_{2.5}$ from

453   reducing SO_2 emissions.

454

455   **6. Conclusions**

456   Standard mechanisms for formation of isoprene secondary organic aerosol (SOA) in

457   chemical transport models assume reversible partitioning of isoprene oxidation products to pre-

458   existing dry OA. This may be appropriate for dry conditions in experimental chambers but not

459   for typical atmospheric conditions where the aerosol is mostly aqueous. Here we developed an

460   aqueous-phase reactive uptake mechanism coupled to a detailed gas-phase isoprene chemistry

461   mechanism to describe the reactive uptake of water-soluble isoprene oxidation products to

462   aqueous aerosol. We applied this mechanism in the GEOS-Chem chemical transport model to

463   simulate surface (SOAS) and aircraft (SEAC^{4}RS) observations over the Southeast US in summer

464   2013.

465   Our mechanism includes different channels for isoprene SOA formation by the high-NO_x

466   pathway, when the isoprene peroxy radicals (ISOPO$_2$) react with NO, and in the low-NO_x

467   pathway where they react mostly with HO$_2$. The main SOA precursors are found to be isoprene

468   epoxide (IEPOX) in the low-NO_x pathway and glyoxal in the high- and low-NO_x pathways. Both

469   of these precursors have dominant gas-phase photochemical sinks, and so their uptake by

470   aqueous aerosol is nearly proportional to the reactive uptake coefficient γ and to the aqueous

471   aerosol mass concentration. The γ for IEPOX is mostly determined by the rate of H$^+$-catalyzed

472   ring opening in the aqueous phase.

473   Application of our mechanism to the Southeast US indicates a mean isoprene SOA yield

474   of 3.3% on a mass basis. By contrast, a conventional mechanism based on reversible uptake of

475   semivolatile isoprene oxidation products yields only 1.1%. Simulation of the observed

476   relationship of OA with formaldehyde (HCHO) provides support for our higher yield. We find

477   that the low-NO_x pathway is 5 times more efficient than the high-NO_x pathway for isoprene SOA

478   production. Under Southeast US conditions, IEPOX and glyoxal account respectively for 58%

479   and 28% of isoprene SOA.

480   Our model simulates well the observations and variability of IEPOX SOA at the surface

481   and from aircraft. The observations show a strong correlation with sulfate that we reproduce in

482   the model. We find this is due to the effect of sulfate on aerosol pH and volume concentration,

483   increasing IEPOX uptake by the H^+-catalyzed ring-opening mechanism. Low concentrations of

484   sulfate are associated with very low IEPOX SOA, both in the observations and the model, and

485   we attribute this to the compounding effects of low sulfate on aerosol $[H^+]$ and on aerosol

486   volume.

487   The US EPA has projected that US NO_x and SO_2 emissions will decrease by 34 and 48%

488   respectively from 2013 to 2025. We find in our model that the NO_x reduction will increase

489   isoprene SOA by 7%, reflecting greater importance of the low-NO_x pathway. The SO_2 reduction

490   will decrease isoprene SOA by 35%, due to decreases in both aerosol $[H^+]$ and volume

491   concentration. The combined effect of these two changes is to decrease isoprene SOA by 32%,

492   corresponding to a decrease in the isoprene SOA mass yield from 3.3% to 2.3%. Decreasing SO_2

493   emissions by 48% has similar relative effects on sulfate (36%) and isoprene SOA (35%).

494   Considering that sulfate presently accounts for about 30% of $PM_{2.5}$ in the Southeast US in

495   summer, while isoprene SOA contributes 25%, we conclude that decreasing isoprene SOA

496   represents a factor of 2 co-benefit when reducing SO_2 emissions.

497

22

512 **References**

513 Anttila, T., Kiendler-Scharr, A., Tillmann, R., and Mentel, T. F.: On the reactive uptake of
514   gaseous compounds by organic-coated aqueous aerosols: Theoretical analysis and
515   application to the heterogeneous hydrolysis of N_2O_5, J. Phys. Chem. A, 110, 10435-10443,
516   doi:10.1021/jp062403c, 2006.

517 Attwood, A. R., Washenfelder, R. A., Brock, C. A., Hu, W., Baumann, K., Campuzano-Jost, P.,
518   Day, D. A., Edgerton, E. S., Murphy, D. M., Palm, B. B., McComiskey, A., Wagner, N. L.,
519   de Sá, S. S., Ortega, A., Martin, S. T., Jimenez, J. L., and Brown, S. S.: Trends in sulfate
520   and organic aerosol mass in the Southeast U.S.: Impact on aerosol optical depth and
521   radiative forcing, Geophys. Res. Lett., 41, 7701-7709, doi:10.1002/2014gl061669, 2014.

522 Bateman, A. P., Bertram, A. K., and Martin, S. T.: Hygroscopic influence on the semisolid-to-
523   liquid transition of secondary organic materials, J. Phys. Chem. A., 119, 4386-4395,
524   doi:10.1021/jp508521c, 2014.

525 Bates, K. H., Crounse, J. D., St Clair, J. M., Bennett, N. B., Nguyen, T. B., Seinfeld, J. H., Stoltz,
526   B. M., and Wennberg, P. O.: Gas phase production and loss of isoprene epoxydiols, J.
527   Phys. Chem. A, 118, 1237-1246, doi:10.1021/jp4107958, 2014.

528 Brégonzio-Rozier, L., Giorio, C., Siekmann, F., Pangui, E., Morales, S. B., Temime-Roussel, B.,
529   Gratien, A., Michoud, V., Cazaunau, M., DeWitt, H. L., Tapparo, A., Monod, A.,
530   and Doussin, J.-F.: Secondary organic aerosol formation from isoprene photooxidation
531   during cloud condensation–evaporation cycles, Atmos. Chem. Phys. Discuss., 15, 20561-
532   20596, doi:10.5194/acpd-15-20561-2015, 2015.

533 Brown, S. S., De Gouw, J. A., Warneke, C., Ryerson, T. B., Dubé, W. P., Atlas, E., Weber, R. J.,
534   Peltier, R. E., Neuman, J. A., Roberts, J. M., Swanson, A., Flocke, F., McKeen, S. A.,
535   Brioude, J., Sommariva, R., Trainer, M., Fehsenfeld, F. C., and Ravishankara, A. R.:
536   Nocturnal isoprene oxidation over the Northeast United States in summer and its impact on
537   reactive nitrogen partitioning and secondary organic aerosol, Atmos. Chem. Phys., 9, 3027-
538   3042, doi:10.5194/acp-9-3027-2009, 2009.

539 Budisulistiorini, S. H., Canagaratna, M. R., Croteau, P. L., Marth, W. J., Baumann, K., Edgerton,
540   E. S., Shaw, S. L., Knipping, E. M., Worsnop, D. R., Jayne, J. T., Gold, A., and Surratt, J.
541   D.: Real-time continuous characterization of secondary organic aerosol derived from
542   isoprene epoxydiols in downtown Atlanta, Georgia, using the Aerodyne aerosol chemical
543   speciation monitor, Environ. Sci. Technol., 47, 5686-5694, doi:10.1021/es400023n, 2013.

544 Budisulistiorini, S. H., Li, X., Bairai, S. T., Renfro, J., Liu, Y., Liu, Y. J., McKinney, K. A.,
545   Martin, S. T., McNeill, V. F., Pye, H. O. T., Nenes. A., Neff, M. E., Stone, E. A., Mueller,
546   S., Knote, C., Shaw, S. L., Zhang, Z., Gold, A., and Surratt, J. D.: Examining the effects of
547   anthropogenic emissions on isoprene-derived secondary organic aerosol formation during
548   the 2013 Southern Oxidant and Aerosol Study (SOAS) at the Look Rock, Tennessee
549   ground site, Atmos. Chem. Phys., 15, 8871-8888, doi:10.5194/acp-15-8871-2015, 2015.

550 Buxton, G. V., Malone, T. N., and Salmon, G. A.: Oxidation of glyoxal initiated by ˙OH in
551   oxygenated aqueous solution, J Chem. Soc. Faraday T., 93, 2889-2891, doi
552   10.1039/A701468f, 1997.

553

554 Canagaratna, M. R., Jayne, J. T., Jimenez, J. L., Allan, J. D., Alfarra, M. R, Zhang, Q., Onasch,
555   T. B., Drewnick, F., Coe, H., Middlebrook, A., Delia, A., Williams, L. R., Trimborn, A.
556   M., Northway, M. J., DeCarlo, P. F., Kolb, C. E., Davidovits, P., Worsnop, D. R.:
557   Chemical and microphysical characterization of ambient aerosols with the Aerodyne
558   Aerosol Mass Spectrometer. Mass Spectrometry Reviews, 26, 185-222, doi:
559   10.1002/mas.20115, 2007.

560 Carlton, A. G., Turpin, B. J., Altieri, K. E., Seitzinger, S. P., Mathur, R., Roselle, S. J., and
561   Weber, R. J.: CMAQ model performance enhanced when in-cloud secondary organic
562   aerosol is included: Comparisons of organic carbon predictions with measurements,
563   Environ. Sci. Technol., 42, 8789–8802, doi:1021/es801192n, 2008.

564 Carlton, A. G., Wiedinmyer, C., and Kroll, J. H.: A review of secondary organic aerosol (SOA)
565   formation from isoprene, Atmos. Chem. Phys., 9, 4987-5005, doi:10.5194/acp-9-4987-
566   2009, 2009.

567 Carlton, A. G., and Turpin, B. J.: Particle partitioning potential of organic compounds is highest
568   in the Eastern US and driven by anthropogenic water, Atmos. Chem. Phys., 13, 10203-
569   10214, doi:10.5194/acp-13-10203-2013, 2013.

570 Cazorla, M., Wolfe, G. M., Bailey, S. A., Swanson, A. K., Arkinson, H. L., and Hanisco, T. F.: A
571   new airborne laser-induced fluorescence instrument for in situ detection of formaldehyde
572   throughout the troposphere and lower stratosphere, Atmos. Meas. Tech., 8, 541-552,
573   doi:10.5194/amt-8-541-2015, 2015.

574 Chan, A. W. H., Chan, M. N., Surratt, J. D., Chhabra, P. S., Loza, C. L., Crounse, J. D., Yee, L.
575   D., Flagan, R. C., Wennberg, P. O., and Seinfeld, J. H.: Role of aldehyde chemistry and
576   NO_x concentrations in secondary organic aerosol formation, Atmos. Chem. Phys., 10,
577   7169-7188, doi:10.5194/acp-10-7169-2010, 2010.

578 Cole-Filipiak, N. C., O'Connor, A. E., and Elrod, M. J.: Kinetics of the hydrolysis of
579   atmospherically relevant isoprene-derived hydroxy epoxides, Environ. Sci. Technol., 44,
580   6718-6723, doi:10.1021/es1019228, 2010.

581 Darer, A. I., Cole-Filipiak, N. C., O'Connor, A. E., and Elrod, M. J.: Formation and stability of
582   atmospherically relevant isoprene-derived organosulfates and organonitrates, Environ. Sci.
583   Technol., 45, 1895-1902, doi:10.1021/es103797z, 2011.

584 DeCarlo, P. F., Kimmel, J. R. Trimborn, A., Northway, M. J., Jayne, J. T., Aiken, A. C., Gonin,
585   M., Fuhrer, K., Horvath, T., Docherty, K. S., Worsnop, D. R., and Jimenez, J. L.: Field-
586   deployable, High-Resolution, Time-of-Flight Aerosol Mass Spectrometer, Anal. Chem., 78,
587   8281-8289, doi: 10.1021/ac061249n, 2006.

588 Dommen, J., Metzger, A., Duplissy, J., Kalberer, M., Alfarra, M. R., Gascho, A., Weingartner,
589   E., Prévôt, A. S. H., Verheggen, B., and Baltensperger, U.: Laboratory observation of
590   oligomers in the aerosol from isoprene/NO_x photooxidation, Geophys. Res. Lett., 33,
591   L13805, doi:10.1029/2006gl026523, 2006.

592 Donahue, N. M., Robinson, A. L., Stanier, C. O., and Pandis, S. N.: Coupled partitioning,
593   dilution, and chemical aging of semivolatile organics, Environ. Sci. Technol., 40, 2635-
594   2643, doi:10.1021/es052297c, 2006.

Drury, E., Jacob, D. J., Spurr, R. J. D., Wang, J., Shinozuka, Y., Anderson, B. E., Clarke, A. D., Dibb, J., McNaughton, C., and Weber, R.: Synthesis of satellite (MODIS), aircraft (ICARTT), and surface (IMPROVE, EPA-AQS, AERONET) aerosol observations over eastern North America to improve MODIS aerosol retrievals and constrain surface aerosol concentrations and sources, J. Geophys. Res., 115, D14204, doi:10.1029/2009jd012629, 2010.

EPA: U. S. Environmental Protection Agency, Technical Support Document (TSD): Preparation of Emissions Inventories for the Version 6.1, 2011 Emissions Modeling Platform, available at: http://www.epa.gov/ttn/chief/emch/2011v6/2011v6.1_2018_2025_base_EmisMod_TSD _nov2014_v6.pdf (Accessed on July 15, 2015), 2014.

Eddingsaas, N. C., VanderVelde, D. G., and Wennberg, P. O.: Kinetics and products of the acid-catalyzed ring-opening of atmospherically relevant butyl epoxy alcohols, J. Phys. Chem. A, 114, 8106-8113, doi:10.1021/jp103907c, 2010.

Edney, E. O., Kleindienst, T. E., Jaoui, M., Lewandowski, M., Offenberg, J. H., Wang, W., and Claeys, M.: Formation of 2-methyl tetrols and 2-methylglyceric acid in secondary organic aerosol from laboratory irradiated isoprene/NO_x/SO_2/air mixtures and their detection in ambient $PM_{2.5}$ samples collected in the eastern United States, Atmos. Environ., 39, 5281-5289, doi:10.1016/j.atmosenv.2005.05.031, 2005.

Ervens, B., Gligorovski, S., and Herrmann, H.: Temperature-dependent rate constants for hydroxyl radical reactions with organic compounds in aqueous solutions, Phys. Chem. Chem. Phys., 5, 1811-1824, doi:10.1039/b300072a, 2003.

Ervens, B., Turpin, B. J., and Weber, R. J.: Secondary organic aerosol formation in cloud droplets and aqueous particles (aqSOA): A review of laboratory, field and model studies, Atmos. Chem. Phys., 11, 11069-11102, doi:10.5194/acp-11-11069-2011, 2011.

Fisher, J. A., Jacob, D., Travis, K. R., Kim, P. S., Marais, E. A., Miller, C. C., Yu, K., Zhu, L., Yantosca, R. M., Sulprizio, M. P., Mao, J., Wennberg, P. O., Crounse, J. D., Teng, A. P., Nguyen, T. B., Cohen, R. C., Romer, P., Nault, B. A., Jimenez, J. L., Campuzano-Jost, P., Shepson, P. B., Xiong, F., Blake, D. R., Goldstein, A. H., Hanisco, T. F., Ryerson, T. B., Wisthaler, A., and Mikoviny, T.: Organic nitrate chemistry and its implications for nitrogen budgets in and isoprene- and monoterpene-rich atmosphere: constraints from aircraft (SEAC[4]RS) and ground-based (SOAS) observations in the Southeast US, in preparation, 2016.

Fountoukis, C., and Nenes, A.: ISORROPIA II: A computationally efficient thermodynamic equilibrium model for K^+-Ca^{2+}-Mg^{2+}-NH_4^+-Na^+-SO_4^{2-}-NO_3^--Cl^--H_2O aerosols, Atmos. Chem. Phys., 7, 4639-4659, doi:10.5194/acp-7-4639-2007, 2007.

Fu, T.-M., Jacob, D. J., Wittrock, F., Burrows, J. P., Vrekoussis, M., and Henze, D. K.: Global budgets of atmospheric glyoxal and methylglyoxal, and implications for formation of secondary organic aerosols, J. Geophys. Res., 113, D15303, doi:10.1029/2007jd009505, 2008.

Fu, T.-M., Jacob, D. J., and Heald, C. L.: Aqueous-phase reactive uptake of dicarbonyls as a source of organic aerosol over eastern North America, Atmos. Environ., 43, 1814-1822, doi:10.1016/j.atmosenv.2008.12.029, 2009.

637 Gaston, C. J., Riedel, T. P., Zhang, Z., Gold, A., Surratt, J. D., and Thornton, J. A.: Reactive
638   uptake of an isoprene-derived epoxydiol to submicron aerosol particles, Environ. Sci.
639   Technol., 48, 11178-11186, doi:10.1021/es5034266, 2014.

640 González Abad, G. G., Liu, X., Chance, K., Wang, H., Kurosu, T. P., and Suleiman, R.: Updated
641   Smithsonian Astrophysical Observatory Ozone Monitoring Instrument (SAO OMI)
642   formaldehyde retrieval, Atmos. Meas. Tech., 8, 19-32, doi:10.5194/amt-8-19-2015, 2015.

643 Guenther, A., Karl, T., Harley, P., Wiedinmyer, C., Palmer, P. I., and Geron, C.: Estimates of
644   global terrestrial isoprene emissions using MEGAN (Model of Emissions of Gases and
645   Aerosols from Nature), Atmos. Chem. Phys., 6, 3181-3210, doi:10.5194/acp-6-3181-2006,
646   2006.

647 Guenther, A. B., Jiang, X., Heald, C. L., Sakulyanontvittaya, T., Duhl, T., Emmons, L. K., and
648   Wang, X.: The Model of Emissions of Gases and Aerosols from Nature version 2.1
649   (MEGAN2.1): An extended and updated framework for modeling biogenic emissions,
650   Geosci. Model Dev., 5, 1471-1492, doi:10.5194/gmd-5-1471-2012, 2012.

651 Guo, H., Xu, L., Bougiatioti, A., Cerully, K. M., Capps, S. L., Hite Jr., J. R., Carlton, A. G., Lee,
652   S.-H., Bergin, M. H., Ng, N. L., Nenes, A., and Weber, R. J.: Fine-particle water and pH in
653   the southeastern United States, Atmos. Chem. Phys., 15, 5211-5228, doi:10.5194/acp-15-
654   5211-2015, 2015.

655 Hallquist, M., Wenger, J. C., Baltensperger, U., Rudich, Y., Simpson, D., Claeys, M., Dommen,
656   J., Donahue, N. M., George, C., Goldstein, A. H., Hamilton, J. F., Herrmann, H.,
657   Hoffmann, T., Iinuma, Y., Jang, M., Jenkin, M. E., Jimenez, J. L., Kiendler-Scharr, A.,
658   Maenhaut, W., McFiggans, G., Mentel, Th. F., Monod, A., Prévôt, A. S. H., Seinfeld, J. H.,
659   Surratt, J. D., Szmigielski, R., and Wildt, J.: The formation, properties and impact of
660   secondary organic aerosol: Current and emerging issues, Atmos. Chem. Phys., 9, 5155-
661   5236, doi:10.5194/acp-9-5155-2009, 2009.

662 Hess, M., Koepke, P., and Schult, I.: Optical properties of aerosols and clouds: The software
663   package OPAC, B. Am. Meteorol. Soc., 79, 831–844, 1998.

664 Hodzic, A., and Jimenez, J. L.: Modeling anthropogenically controlled secondary organic
665   aerosols in a megacity: A simplified framework for global and climate models, Geosci.
666   Model. Dev., 4, 901-917, doi:10.5194/gmd-4-901-2011, 2011.

667 Hu, K. S., Darer, A. I., and Elrod, M. J.: Thermodynamics and kinetics of the hydrolysis of
668   atmospherically relevant organonitrates and organosulfates, Atmos. Chem. Phys., 11, 8307-
669   8320, doi:10.5194/acp-11-8307-2011, 2011.

670 Hu, W. W., Campuzano-Jost, P., Palm, B. B., Day, D. A., Ortega, A. M., Hayes, P. L.,
671   Krechmer, J. E., Chen, Q., Kuwata, M., Liu, Y. J., de Sá, S. S., Martin, S. T., Hu, M.,
672   Budisulistiorini, S. H., Riva, M., Surratt, J. D., St. Clair, J. M., Isaacman-Van Wertz, G.,
673   Yee, L. D., Goldstein, A. H., Carbone, S., Artaxo, P., de Gouw, J. A., Koss, A., Wisthaler,
674   A., Mikoviny, T., Karl, T., Kaser, L., Jud, W., Hansel, A. Docherty, K. S., Robinson, N. H.,
675   Coe, H., Allan, J. D., Canagaratna, M. R., Paulot, F., and Jimenez, J. L.: Characterization
676   of a real-time tracer for isoprene epoxydiols-derived secondary organic aerosol (IEPOX-
677   SOA) from aerosol mass spectrometer measurements, Atmos. Chem. Phys., 15, 11807–
678   11833, doi:10.5194/acp-15-11807-2015, 2015.

679 Jacob, D. J.: Heterogeneous chemistry and tropospheric ozone, Atmos. Environ., 34, 2131-2159,
680   doi:10.1016/s1352-2310(99)00462-8, 2000.

681 Jacobs, M. I., Darer, A. I., and Elrod, M. J.: Rate constants and products of the OH reaction with
682   isoprene-derived epoxides, Environ. Sci. Technol., 47, 12868-12876,
683   doi:10.1021/es403340g, 2013.

684 Jacobs, M. I., Burke, W. J., and Elrod, M. J.: Kinetics of the reactions of isoprene-derived
685   hydroxynitrates: Gas phase epoxide formation and solution phase hydrolysis, Atmos.
686   Chem. Phys., 14, 8933-8946, doi:10.5194/acp-14-8933-2014, 2014.

687 Kim, P. S., Jacob, D. J., Fisher, J. A., Travis, K., Yu, K., Zhu, L., Yantosca, R. M., Sulprizio, M.
688   P., Jimenez, J. L., Campuzano-Jost, P., Froyd, K. D., Liao, J., Hair, J. W., Fenn, M. A.,
689   Butler, C. F., Wagner, N. L., Gordon, T. D., Welti, A., Wennberg, P. O., Crounse, J. D., St.
690   Clair, J. M., Teng, A. P., Millet, D. B., Schwarz, J. P., Markovic M. Z., and Perring, A. E.:
691   Sources, seasonality, and trends of southeast US aerosol: an integrated analysis of surface,
692   aircraft, and satellite observations with the GEOS-Chem chemical transport model, Atmos.
693   Chem. Phys, 15, 10411-10433, doi:10.5194/acpd-15-10411-2015, 2015.

694 King, S. M., Rosenoern, T., Shilling, J. E., Chen, Q., Wang, Z., Biskos, G., McKinney, K. A.,
695   Pöschl, U., and Martin, S. T.: Cloud droplet activation of mixed organic-sulfate particles
696   produced by the photooxidation of isoprene, Atmos. Chem. Phys., 10, 3953-3964,
697   doi:10.5194/acp-10-3953-2010, 2010.

698 Kleindienst, T. E., Edney, E. O., Lewandowski, M., Offenberg, J. H., and Jaoui, M.: Secondary
699   organic carbon and aerosol yields from the irradiations of isoprene and α-pinene in the
700   presence of NO_x and SO_2, Environ. Sci. Technol., 40, 3807-3812, doi:10.1021/es052446r,
701   2006.

702 Kleindienst, T. E., Lewandowski, M., Offenberg, J. H., Jaoui, M., and Edney, E. O.: Ozone-
703   isoprene reaction: Re-examination of the formation of secondary organic aerosol, Geophys.
704   Res. Lett., 34, L01805, doi:10.1029/2006gl027485, 2007.

705 Kleindienst, T. E., Lewandowski, M., Offenberg, J. H., Jaoui, M., and Edney, E. O.: The
706   formation of secondary organic aerosol from the isoprene + OH reaction in the absence of
707   NO_x, Atmos. Chem. Phys., 9, 6541-6558, doi:10.5194/acp-9-6541-2009, 2009.

708 Knote, C., Hodzic, A., Jimenez, J. L., Volkamer, R., Orlando, J. J., Baidar, S., Brioude, J., Fast,
709   J., Gentner, D. R., Goldstein, A. H., Hayes, P. L., Knighton, W. B., Oetjen, H., Setyan, A.,
710   Stark, H., Thalman, R., Tyndall, G., Washenfelder, R., Waxman, E., and Zhang, Q.:
711   Simulation of semi-explicit mechanisms of SOA formation from glyoxal in aerosol in a 3-
712   D model, Atmos. Chem. Phys., 14, 6213-6239, doi:10.5194/acp-14-6213-2014, 2014.

713 Koepke, P., Hess, M., Schult, I., and Shettle, E. P.: Global aerosol data set, report, Max-Planck
714   Inst. für Meteorol., Hamburg, Germany, 1997.

715 Krechmer, J. E., Coggon, M. M., Massoli, P., Nguyen, T. B., Crounse, J. D., Hu, W., Day, D. A.,
716   Tyndall, G. S., Henze, D. K., Rivera-Rios, J. C., Nowak, J. B., Kimmel, J. R., Mauldin, III,
717   R. L., Stark, H., Jayne, J. T., Sipilä, M., Junninen, H., St. Clair, J. M., Zhang, X., Feiner, P.
718   A., Zhang, L., Miller, D. O., Brune, W. H., Keutsch, F. N., Wennberg, P. O., Seinfeld, J.
719   H., Worsnop, D. R., Jimenez, J. L., and Canagaratna, M. R.: Formation of low volatility
720   organic compounds and secondary organic aerosol from isoprene hydroxyhydroperoxide

low-NO oxidation, Environ. Sci. Technol., 49, 10330-10339, doi:10.1021/acs.est.5b02031, 2015.

Kroll, J. H., Ng, N. L., Murphy, S. M., Flagan, R. C., and Seinfeld, J. H.: Secondary organic aerosol formation from isoprene photooxidation under high-NO_x conditions, Geophys. Res. Lett., 32, L18808, doi:10.1029/2005gl023637, 2005.

Kroll, J. H., Ng, N. L., Murphy, S. M., Flagan, R. C., and Seinfeld, J. H.: Secondary organic aerosol formation from isoprene photooxidation, Environ. Sci. Technol., 40, 1869-1877, doi:10.1021/es0524301, 2006.

Lee, L., Teng, A. P., Wennberg, P. O., Crounse, J. D., and Cohen, R. C.: On rates and mechanisms of OH and O_3 reactions with isoprene-derived hydroxy nitrates, J. Phys. Chem. A, 118, 1622-1637, doi:10.1021/jp4107603, 2014.

Lewandowski, M., Jaoui, M., Offenberg, J. H., Krug, J. D., and Kleindienst, T. E.: Atmospheric oxidation of isoprene and 1,3-butadiene: Influence of aerosol acidity and relative humidity on secondary organic aerosol, Atmos. Chem. Phys., 15, 3773-3783, doi:10.5194/acp-15-3773-2015, 2015.

Liao, J., Froyd, K. D., Murphy, D. M., Keutsch, F. N., Yu, G., Wennberg, P. O., St Clair, J. M., Crounse, J. D., Wisthaler, A., Mikoviny, T., Jimenez, J. L., Campuzano-Jost, P., Day, D. A., Hu, W., Ryerson, T. B., Pollack, I. B., Peischl, J., Anderson, B. E., Ziemba, L. D., Blake, D. R., Meinardi, S., and Diskin, G.: Airborne measurements of organosulfates over the continental U.S., J. Geophys. Res., 120, 2990-3005, doi:10.1002/2014jd022378, 2015.

Liggio, J., Li, S.-M., and McLaren, R.: Reactive uptake of glyoxal by particulate matter, J. Geophys. Res., 110, D10304, doi:10.1029/2004jd005113, 2005.

Lin, Y.-H., Zhang, H., Pye, H. O. T., Zhang, Z. F., Marth, W. J., Park, S., Arashiro, M., Cui, T., Budisulistiorini, S. H., Sexton, K. G., Vizuete, W., Xie, Y., Luecken, D. J., Piletic, I. R., Edney, E. O., Bartolotti, L. J., Gold, A., and Surratt, J. D.: Epoxide as a precursor to secondary organic aerosol formation from isoprene photooxidation in the presence of nitrogen oxides, P. Natl. Acad. Sci. USA, 110, 6718-6723, doi:10.1073/pnas.1221150110, 2013.

Liu, Y. J., Herdlinger-Blatt, I., McKinney, K. A., and Martin, S. T.: Production of methyl vinyl ketone and methacrolein via the hydroperoxyl pathway of isoprene oxidation, Atmos. Chem. Phys., 13, 5715-5730, doi:10.5194/acp-13-5715-2013, 2013.

Lin, G., S. Sillman, J. E. Penner, and A. Ito, Global modeling of SOA: the use of different mechanisms for aqueous-phase formation, Atmos. Chem. Phys., 14, 5451-5475, doi:10.5194/acp-14-5451-2014, 2014.

Liu, J., L. W. Horowitz, S. Fan, A. G. Carlton, and H. Levy II, Global in-cloud production of secondary organic aerosols: implementation of a detailed chemical mechanism in the GFDL atmospheric model AM3, J. Geophys. Res., D117, D15303, doi:10.1029/2012JD017838, 2012.

Mao, J., Paulot, F., Jacob, D. J., Cohen, R. C., Crounse, J. D., Wennberg, P. O., Keller, C. A., Hudman, R. C., Barkley, M. P., and Horowitz, L. W.: Ozone and organic nitrates over the eastern United States: Sensitivity to isoprene chemistry, J. Geophys. Res., 118, 11256-11268, doi:10.1002/jgrd.50817, 2013.

763 Martin, R. V., Jacob, D. J., Yantosca, R. M., Chin, M., and Ginoux, P.: Global and regional
764   decreases in tropospheric oxidants from photochemical effects of aerosols, J. Geophys.
765   Res., 108, 4097, doi:10.1029/2002jd002622, 2003.

766 McNeill, V. F., Woo, J. L., Kim, D. D., Schwier, A. N., Wannell, N. J., Sumner, A. J., and
767   Barakat, J. M.: Aqueous-phase secondary organic aerosol and organosulfate formation in
768   atmospheric aerosols: A modeling study, Environ. Sci. Technol., 46, 8075-8081,
769   doi:10.1021/es3002986, 2012.

770 McNeill, V. F., Sareen, N., and Schwier, A. N.: Surface-active organics in atmospheric aerosols,
771   Top. Curr. Chem., 339, 201-259, doi:10.1007/128_2012_404, 2014.

772 Millet, D. B., Jacob, D. J., Turquety, S., Hudman, R. C., Wu, S., Fried, A., Walega, J., Heikes, B.
773   G., Blake, D. R., Singh, H. B., Anderson, B. E., and Clarke, A. D.: Formaldehyde
774   distribution over North America: Implications for satellite retrievals of formaldehyde
775   columns and isoprene emission, J. Geophys. Res., 111, D24S02,
776   doi:10.1029/2005jd006853, 2006.

777 Myriokefalitakis, S., Tsigaridas, K., Mihalopoulos, N., Sciare, J., Nenes, A., Kawamura, K.,
778   Segers, A., and Kanakidou, M.: In-cloud oxalate formation in the global troposphere: a 3-D
779   modeling study, Atmos. Chem. Phys., 11, 5761-5782, doi:10.5194/acp-11-5761-2011,
780   2011.

781 Ng, N. L., Kwan, A. J., Surratt, J. D., Chan, A. W. H., Chhabra, P. S., Sorooshian, A., Pye, H. O.
782   T., Crounse, J. D., Wennberg, P. O., Flagan, R. C., and Seinfeld, J. H.: Secondary organic
783   aerosol (SOA) formation from reaction of isoprene with nitrate radicals (NO_3), Atmos.
784   Chem. Phys., 8, 4117-4140, doi:10.5194/acp-8-4117-2008, 2008.

785 Nguyen, T. B., Coggon, M. M., Bates, K. H., Zhang, X., Schwantes, R. H., Schilling, K. A.,
786   Loza, C. L., Flagan, R. C., Wennberg, P. O., and Seinfeld, J. H.: Organic aerosol formation
787   from the reactive uptake of isoprene epoxydiols (IEPOX) onto non-acidified inorganic
788   seeds, Atmos. Chem. Phys., 14, 3497-3510, doi:10.5194/acp-14-3497-2014, 2014.

789 Nguyen, T. B., Crounse, J. D., Teng, A. P., St. Clair, J. M., Paulot, F., Wolfe, G. M., and
790   Wennberg, P. O.: Rapid deposition of oxidized biogenic compounds to a temperate forest,
791   P. Natl. Acad. Sci. USA, 112, E392-E401, doi:10.1073/pnas.1418702112, 2015a.

792 Nguyen, T. B., Bates, K. H., Crounse, J. D., Schwantes, R. H., Zhang, X., Kjaergaard, H. G.,
793   Surratt, J. D., Lin, P., Laskin, A., Seinfeld, J. H., and Wennberg, P. O.: Mechanism of the
794   hydroxyl radical oxidation of methacryloyl peroxynitrate (MPAN) and its pathway toward
795   secondary organic aerosol formation in the atmosphere, Phys Chem Chem Phys, 17, 17914-
796   17926, doi:10.1039/c5cp02001h, 2015b.

797 Nozière, B., Dziedzic, P., and Córdova, A.: Products and kinetics of the liquid-phase reaction of
798   glyoxal catalyzed by ammonium ions (NH_4^+), J. Phys. Chem. A, 113, 231-237,
799   doi:10.1021/jp8078293, 2009.

800 Odum, J. R., Hoffmann, T., Bowman, F., Collins, D., Flagan, R. C., and Seinfeld, J. H.:
801   Gas/particle partitioning and secondary organic aerosol yields, Environ. Sci. Technol., 30,
802   2580-2585, doi:10.1021/es950943+, 1996.

803   Palmer, P. I., Jacob, D. J., Fiore, A. M., Martin, R. V., Chance, K., and Kurosu, T. P.: Mapping
804   isoprene emissions over North America using formaldehyde column observations from
805   space, J. Geophys. Res., 108, 4180, doi:10.1029/2002jd002153, 2003.

806   Palmer, P. I., Abbot, D. S., Fu, T.-M., Jacob, D. J., Chance, K., Kurosu, T. P., Guenther, A.,
807   Wiedinmyer, C., Stanton, J. C., Pilling, M. J., Pressley, S. N., Lamb, B., and Sumner, A. L.:
808   Quantifying the seasonal and interannual variability of North American isoprene emissions
809   using satellite observations of the formaldehyde column, J. Geophys. Res., 111, D12315,
810   doi:10.1029/2005jd006689, 2006.

811   Paulot, F., Crounse, J. D., Kjaergaard, H. G., Kroll, J. H., Seinfeld, J. H., and Wennberg, P. O.:
812   Isoprene photooxidation: New insights into the production of acids and organic nitrates,
813   Atmos. Chem. Phys., 9, 1479-1501, doi:10.5194/acp-9-1479-2009, 2009a.

814   Paulot, F., Crounse, J. D., Kjaergaard, H. G., Kürten, A., St Clair, J. M., Seinfeld, J. H., and
815   Wennberg, P. O.: Unexpected epoxide formation in the gas-phase photooxidation of
816   isoprene, Science, 325, 730-733, doi:10.1126/science.1172910, 2009b.

817   Peeters, J., Nguyen, T. L., and Vereecken, L.: HO_x radical regeneration in the oxidation of
818   isoprene, Phys. Chem. Chem. Phys., 11, 5935-5939, doi:10.1039/b908511d, 2009.

819   Peeters, J., and Müller, J.-F.: HO_x radical regeneration in isoprene oxidation via peroxy radical
820   isomerisations. II: Experimental evidence and global impact, Phys. Chem. Chem. Phys., 12,
821   14227-14235, doi:10.1039/c0cp00811g, 2010.

822   Piletic, I. R., Edney, E. O., and Bartolotti, L. J.: A computational study of acid catalyzed aerosol
823   reactions of atmospherically relevant epoxides, Phys. Chem. Chem. Phys., 15, 18065-
824   18076, doi:10.1039/c3cp52851k, 2013.

825   Pye, H. O. T., Chan, A. W. H., Barkley, M. P., and Seinfeld, J. H.: Global modeling of organic
826   aerosol: The importance of reactive nitrogen (NO_x and NO_3), Atmos. Chem. Phys., 10,
827   11261-11276, doi:10.5194/acp-10-11261-2010, 2010.

828   Pye, H. O. T., Pinder, R. W., Piletic, I. R., Xie, Y., Capps, S. L., Lin, Y.-H., Surratt, J. D., Zhang,
829   Z., Gold, A., Luecken, D. J., Hutzell, W. T., Jaoui, M., Offenberg, J. H., Kleindienst, T. E.,
830   Lewandowski, M., and Edney, E. O.: Epoxide pathways improve model predictions of
831   isoprene markers and reveal key role of acidity in aerosol formation, Environ. Sci.
832   Technol., 47, 11056-11064, doi:10.1021/es402106h, 2013.

833   Riedel, T. P., Lin, Y.-H., Budisulistiorini, S. H., Gaston, C. J., Thornton, J. A., Zhang, Z. F.,
834   Vizuete, W., Gold, A., and Surratt, J. D.: Heterogeneous reactions of isoprene-derived
835   epoxides: Reaction probabilities and molar secondary organic aerosol yield estimates,
836   Environ. Sci. Technol. Lett., 2, 38-42, doi:10.1021/ez500406f, 2015.

837   Rollins, A. W., Kiendler-Scharr, A., Fry, J. L., Brauers, T., Brown, S. S., Dorn, H.-P., Dubé, W.
838   P., Fuchs, H., Mensah, A., Mentel, T. F., Rohrer, F., Tillmann, R., Wegener, R.,
839   Wooldridge, P. J., and Cohen, R. C.: Isoprene oxidation by nitrate radical: Alkyl nitrate and
840   secondary organic aerosol yields, Atmos. Chem. Phys., 9, 6685-6703, doi:10.5194/acp-9-
841   6685-2009, 2009.

842   SEAC[4]RS Archive, doi:10.5067/Aircraft/SEAC4RS/Aerosol-TraceGas-Cloud.

843   Sato, K., Nakao, S., Clark, C. H., Qi, L., and Cocker III, D. R.: Secondary organic aerosol
844   formation from the photooxidation of isoprene, 1,3-butadiene, and 2,3-dimethyl-1,3-
845   butadiene under high NO_x conditions, Atmos. Chem. Phys., 11, 7301-7317,
846   doi:10.5194/acp-11-7301-2011, 2011.

847   Saxena, P., and Hildemann, L. M.: Water-soluble organics in atmospheric particles: A critical
848   review of the literature and application of thermodynamics to identify candidate
849   compounds, J. Atmos. Chem., 24, 57-109, doi:10.1007/bf00053823, 1996.

850   Schwartz, S.E.: Mass-transport considerations pertinent to aqueous-phase reactions of gases in
851   liquid-water clouds. In: Jaechske, W. (Ed.), Chemistry of Multiphase Atmospheric
852   Systems, Springer, Heidelberg, pp. 415-471, 1986.

853   Scott, C. E., Rap, A., Spracklen, D. V., Forster, P. M., Carslaw, K. S., Mann, G. W., Pringle, K.
854   J., Kivekäs, N., Kulmala, M., Lihavainen, H., and Tunved, P.: The direct and indirect
855   radiative effects of biogenic secondary organic aerosol, Atmos. Chem. Phys., 14, 447-470,
856   doi:10.5194/acp-14-447-2014, 2014.

857   Song, M., Liu, P. F., Hanna, S. J., Li, Y. J., Martin, S. T., and Bertram, A. K.: Relative humidity-
858   dependent viscosities of isoprene-derived secondary organic material and atmospheric
859   implications for isoprene-dominant forests, Atmos. Chem. Phys., 15, 5145-5159,
860   doi:10.5194/acp-15-5145-2015, 2015.

861   Stavrakou, T., Peeters, J., and Müller, J.-F.: Improved global modelling of HO_x recycling in
862   isoprene oxidation: Evaluation against the GABRIEL and INTEX-A aircraft campaign
863   measurements, Atmos. Chem. Phys., 10, 9863-9878, doi:10.5194/acp-10-9863-2010, 2010.

864   St. Clair, J. M., Rivera-Rios, J. C., Crounse, J. D., Knap, H. C., Bates, K. H., Teng, A. P.,
865   Jørgensen, S., Kjaergaard, H. G., Keutsch, F. N., Wennberg, P. O.: Kinetics and products
866   of the reaction of the first-generation isoprene hydroperoxide (ISOPOOH) with OH, J.
867   Phys. Chem. A, doi:10.1021/acs.jpca.5b06532, 2016.

868   Sumner, A. J., Woo, J. L., and McNeill, V. F.: Model Analysis of secondary organic aerosol
869   formation by glyoxal in laboratory studies: The case for photoenhanced chemistry,
870   Environ. Sci. Technol., 48, 11919-11925, doi:10.1021/es502020j, 2014.

871   Surratt, J. D., Murphy, S. M., Kroll, J. H., Ng, N. L., Hildebrandt, L., Sorooshian, A.,
872   Szmigielski, R., Vermeylen, R., Maenhaut, W., Claeys, M., Flagan, R. C., and Seinfeld, J.
873   H.: Chemical composition of secondary organic aerosol formed from the photooxidation of
874   isoprene, J. Phys. Chem. A, 110, 9665-9690, doi:10.1021/jp061734m, 2006.

875   Surratt, J. D., Lewandowski, M., Offenberg, J. H., Jaoui, M., Kleindienst, T. E., Edney, E. O.,
876   and Seinfeld, J. H.: Effect of acidity on secondary organic aerosol formation from isoprene,
877   Environ. Sci. Technol., 41, 5363-5369, doi:10.1021/es0704176, 2007a.

878   Surratt, J. D., Kroll, J. H., Kleindienst, T. E., Edney, E. O., Claeys, M., Sorooshian, A., Ng, N.
879   L., Offenberg, J. H., Lewandowski, M., Jaoui, M., Flagan, R. C., and Seinfeld, J. H.:
880   Evidence for organosulfates in secondary organic aerosol, Environ. Sci. Technol., 41, 517-
881   527, doi:10.1021/es062081q, 2007b.

882   Surratt, J. D., Chan, A. W. H., Eddingsaas, N. C., Chan, M., Loza, C. L., Kwan, A. J., Hersey, S.
883   P., Flagan, R. C., Wennberg, P. O., and Seinfeld, J. H.: Reactive intermediates revealed in

884 secondary organic aerosol formation from isoprene, P. Natl. Acad. Sci. USA, 107, 6640-
885 6645, doi:10.1073/pnas.0911114107, 2010.

886 Tan, Y., Perri, M. J., Seitzinger, S. P., and Turpin, B. J.: Effects of precursor concentration and
887 acidic sulfate in aqueous glyoxal-OH radical oxidation and implications for secondary
888 organic aerosol, Environ. Sci. Technol., 43, 8105-8112, doi:10.1021/es901742f, 2009.

889 Tan, Y., Carlton, A. G., Seitzinger, S. P., and Turpin, B. J.: SOA from methylglyoxal in clouds
890 and wet aerosols: Measurement and prediction of key products, Atmos. Environ., 44, 5218-
891 5226, doi:10.1016/j.atmosenv.2010.08.045, 2010.

892 Toon, O. B. and the SEAC[4]RS science team: Planning, implementation, and scientific goals of
893 the Studies of Emissions and Atmospheric Composition, Clouds, and Climate Coupling by
894 Regional Surveys (SEAC[4]RS) field mission, submitted to J. Geophys. Res., 2016.

895 Travis, K. R., Jacob, D. J., Fisher, J. A., Kim, P. S., Marais, E. A., Zhu, L., Miller, C. C.,
896 Wennberg, P. O., Crounse, J., Hanisco, T. A., Ryerson, T., Yu, K., Wolfe, G. M.,
897 Thompson, A., Mao, J., Paulot, F., Yantosca, R. M., Sulprizio, M., and Neuman, A.: NO_x
898 emissions, isoprene oxidation pathways, and implications for surface ozone in the
899 Southeast United States, in preparation, 2016.

900 Virtanen, A., Joutsensaari, J., Koop, T., Kannosto, J., Yli-Pirilä, P., Leskinen, J., Mäkelä, J. M.,
901 Holopainen, J. K., Pöschl, U., Kulmala, M., Worsnop, D. R., and Laaksonen, A.: An
902 amorphous solid state of biogenic secondary organic aerosol particles, Nature, 467, 824-
903 827, doi:10.1038/nature09455, 2010.

904 Volkamer, R., Martini, F. S., Molina, L. T., Salcedo, D., Jimenez, J. L., and Molina, M. J.: A
905 missing sink for gas-phase glyoxal in Mexico City: Formation of secondary organic
906 aerosol, Geophys. Res. Lett., 34, L19807, doi:10.1029/2007gl030752, 2007.

907 Volkamer, R., Ziemann, P. J., and Molina, M. J.: Secondary organic aerosol formation from
908 acetylene (C_2H_2): Seed effect on SOA yields due to organic photochemistry in the aerosol
909 aqueous phase, Atmos. Chem. Phys., 9, 1907-1928, doi:10.5194/acp-9-1907-2009, 2009.

910 Wagner, N. L., Brock, C. A., Angevine, W. M., Beyersdorf, A., Campuzano-Jost, P., Day, D., de
911 Gouw, J. A., Diskin, G. S., Gordon, T. D., Graus, M. G., Holloway, J. S., Huey, G.,
912 Jimenez, J. L., Lack, D. A., Liao, J., Liu, X., Markovic, M. Z., Middlebrook, A. M.,
913 Mikoviny, T., Peischl, J., Perring, A. E., Richardson, M. S., Ryerson, T. B., Schwarz, J. P.,
914 Warneke, C., Welti, A., Wisthaler, A., Ziemba, L. D., and Murphy, D. M.: In situ vertical
915 profiles of aerosol extinction, mass, and composition over the southeast United States
916 during SENEX and SEAC[4]RS: Observations of a modest aerosol enhancement aloft,
917 Atmos. Chem. Phys., 15, 7085-7102, doi:10.5194/acp-15-7085-2015, 2015.

918 Wang, J., Hoffmann, A. A., Park, R. J., Jacob, D. J., and Martin, S. T.: Global distribution of
919 solid and aqueous sulfate aerosols: Effect of the hysteresis of particle phase transitions, J.
920 Geophys. Res., 113, D11206, doi:10.1029/2007jd009367, 2008.

921 Waxman, E. M., Dzepina, K., Ervens, B., Lee-Taylor, J., Aumont, B., Jimenez, J. L., Madronich,
922 S., and Volkamer, R.: Secondary organic aerosol formation from semi- and intermediate-
923 volatility organic compounds and glyoxal: Relevance of O/C as a tracer for aqueous
924 multiphase chemistry, Geophys. Res. Lett., 40, 978-982, doi:10.1002/grl.50203, 2013.

925 Xu, L., Kollman, M. S., Song, C., Shilling, J. E., and Ng, N. L.: Effects of NO_x on the volatility
926   of secondary organic aerosol from isoprene photooxidation, Environ. Sci. Technol., 48,
927   2253-2262, doi:10.1021/es404842g, 2014.

928 Xu, L., Guo, H., Boyd, C. M., Klein, M., Bougiatioti, A., Cerully, K. M., Hite, J. R., Isaacman-
929   VanWertz, G., Kreisberg, N. M., Knote, C., Olson, K., Koss, A., Goldstein, A. H., Hering,
930   S. V., de Gouw, J., Baumann, K., Lee, S.-H., Nenes, A., Weber, R. J., and Ng, N. L.:
931   Effects of anthropogenic emissions on aerosol formation from isoprene and monoterpenes
932   in the southeastern United States, P. Natl. Acad. Sci. USA, 112, 37-42,
933   doi:10.1073/pnas.1417609112, 2015.

934 Yu, K., Jacob, D. J., Fisher, J., Kim, P. S., Marais, E. A., Miller, C. C., Travis, K., Zhu, L.,
935   Yantosca, R. M., Sulprizio, M., Cohen, R. C., Dibb, J. E., Fried, A., Mikoviny, T., Ryerson,
936   T. B., Wennberg, P. O., and Wisthaler, A.: Sensitivity to grid resolution in the ability of a
937   chemical transport model to simulate observed oxidant chemistry under high-isoprene
938   conditions, submitted to Atmos. Chem. Phys., 2016.

939 Zhang, Q., Jimenez, J. L., Canagaratna, M. R., Allan, J. D., Coe, H., Ulbrich, I., Alfarra, M. R.,
940   Takami, A., Middlebrook, A. M., Sun, Y. L., Dzepina, K., Dunlea, E., Docherty, K.,
941   DeCarlo, P. F., Salcedo, D., Onasch, T., Jayne, J. T., Miyoshi, T., Shimono, A.,
942   Hatakeyama, S., Takegawa, N., Kondo, Y., Schneider, J., Drewnick, F., Borrmann, S.,
943   Weimer, S., Demerjian, K., Williams, P., Bower, K., Bahreini, R., Cottrell, L., Griffin, R.
944   J., Rautiainen, J., Sun, J. Y., Zhang, Y. M., and Worsnop, D. R.: Ubiquity and dominance
945   of oxygenated species in organic aerosols in anthropogenically-influenced Northern
946   Hemisphere midlatitudes, Geophys. Res. Lett., 34, L13801, doi:10.1029/2007gl029979,
947   2007.

948 Zhang, H., Surratt, J. D., Lin, Y. H., Bapat, J., and Kamens, R. M.: Effect of relative humidity on
949   SOA formation from isoprene/NO photooxidation: Enhancement of 2-methylglyceric acid
950   and its corresponding oligoesters under dry conditions, Atmos. Chem. Phys., 11, 6411-
951   6424, doi:10.5194/acp-11-6411-2011, 2011.

952 Zhang, H., Parikh, H. M., Bapat, J., Lin, Y. H., Surratt, J. D., and Kamens, R. M.: Modelling of
953   secondary organic aerosol formation from isoprene photooxidation chamber studies using
954   different approaches, Environ. Chem., 10, 194-209, doi:10.1071/en13029, 2013.

955 Zhu, L., Jacob, D., Mickley, L., Kim, P. S., Fisher, J., Travis, K., Yu, K., Yantosca, R. M.,
956   Sulprizio, M., Fried, A., Hanisco, T., Wolfe, G., Abad, G. G., Chance, K., De Smedt, I.,
957   and Yang, K.: Indirect validation of new OMI, GOME-2, and OMPS formaldehyde
958   (HCHO) retrievals using SEAC[4]RS data, in preparation, 2016.

959 **TABLES**

960 **Table 1.** Constants for reactive uptake of isoprene SOA precursors [a]

Species [b]	H^* [M atm^{-1}]	k_{H+} [M^{-1} s^{-1}]	k_{nuc} [M^{-2} s^{-1}]	k_{HSO4-} [M^{-1} s^{-1}]	k_{aq} [s^{-1}]
IEPOX	3.3×10^{7}, [c]	3.6×10^{-2}, [d]	2.0×10^{-4}, [e]	7.3×10^{-4}, [e]	Equation (2)
ISOPN$_\beta$ [f]	3.3×10^{5}, [g]	–	–	–	1.6×10^{-5}, [h]
ISOPN$_\delta$ [f]	3.3×10^{5}, [g]	–	–	–	6.8×10^{-3}, [h]
DHDN	3.3×10^{5}, [g]	–	–	–	6.8×10^{-3}, [i]

961 [a] Effective Henry's law constants H^* and aqueous-phase rate constants used to calculate reactive uptake
962 coefficients γ for isoprene SOA precursors IEPOX, ISOPN$_\beta$, ISOPN$_\delta$, and DHDN following Eqs. (1) and
963 (2). Calculation of γ for other isoprene SOA precursors in Fig. 2 is described in the text.

964 [b] See Fig. 2 for definition of acronyms.

965 [c] Best fit to SOAS and SEAC^{4}RS IEPOX SOA and consistent with Nguyen et al. (2014).

966 [d] Cole-Filipiak et al. (2010).

967 [e] Eddingsaas et al. (2010).

968 [f] ISOPN species formed from the beta and delta isoprene oxidation channels (Paulot et al., 2009a) are
969 treated separately in GEOS-Chem.

970 [g] By analogy with 4-nitrooxy-3-methyl-2-butanol (Rollins et al., 2009).

971 [h] Jacobs et al. (2014).

972 [i] Assumed same as for ISOPN$_\delta$ (Hu et al., 2011).

973   **Table 2.** Mean reactive uptake coefficients γ of isoprene SOA precursors [a]

Species [b]	γ	pH dependence [c]			
		pH > 3	2 < pH < 3	1 < pH < 2	0 < pH < 1
IEPOX	4.2×10^{-3}	8.6×10^{-7}	2.0×10^{-4}	1.1×10^{-3}	1.0×10^{-2}
MEPOX	1.3×10^{-4}	2.7×10^{-8}	6.4×10^{-6}	3.6×10^{-5}	3.2×10^{-4}
ISOPN$_\beta$	1.3×10^{-7}	–			
ISOPN$_\delta$	5.2×10^{-5}	–			
DHDN	6.5×10^{-5}	–			
GLYX	$2.9 \times 10^{-3, \, d}$	–			
MGLY	4.0×10^{-7}	–			
C$_5$-LVOC	0.1	–			
NT-ISOPN	0.1	–			

974   [a] Mean values computed in GEOS-Chem for the Southeast US in summer as sampled along the boundary-
975   layer (< 2 km) SEAC[4]RS aircraft tracks and applied to aqueous aerosol. The reactive uptake coefficient γ
976   is defined as the probability that a gas molecule colliding with an aqueous aerosol particle will be taken
977   up and react in the aqueous phase to form non-volatile products.

978   [b] See Fig. 2 for definition of acronyms.

979   [c] γ for IEPOX and MEPOX are continuous functions of pH (Eq. (2)). Values shown here are averages for
980   different pH ranges sampled along the SEAC[4]RS flight tracks. Aqueous aerosol pH is calculated locally
981   in GEOS-Chem using the ISORROPIA thermodynamic model (Fountoukis and Nenes, 2007).

982   [d] Daytime value. Nighttime value is 5×10^{-6}.

983

FIGURES

985
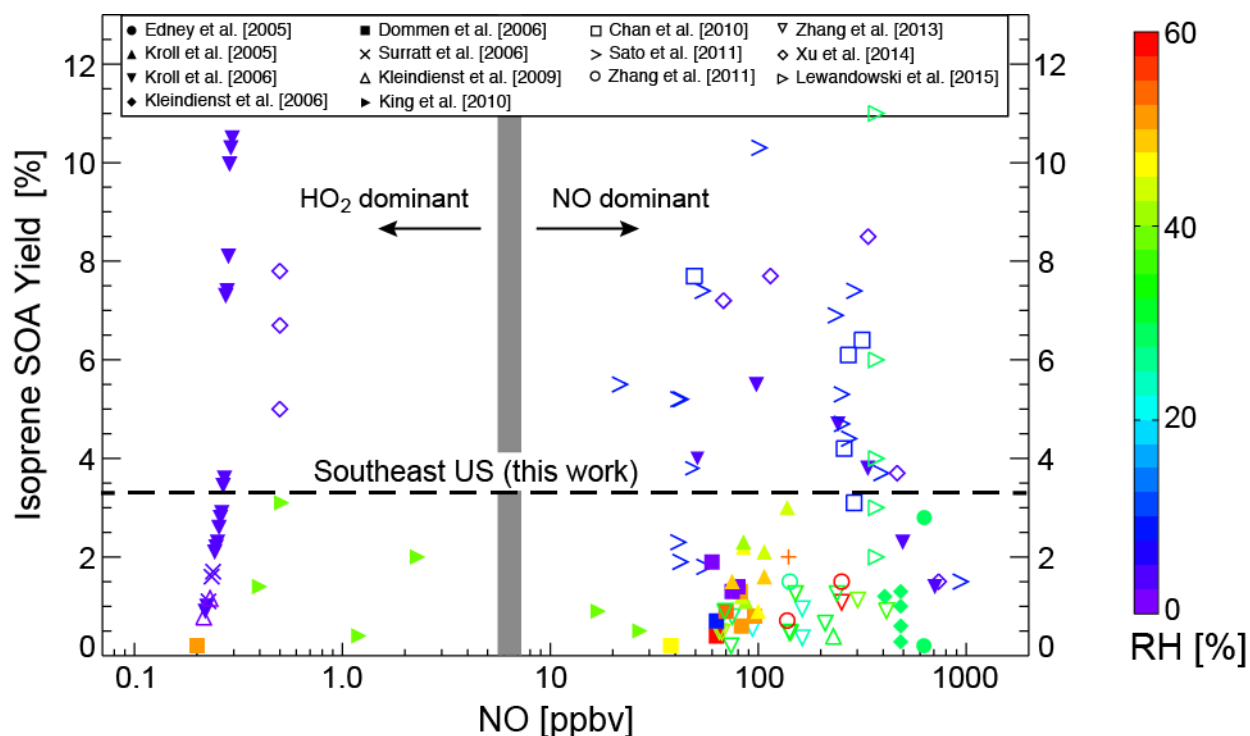
986

987

988   **Figure 1.** Yields of secondary organic aerosol (SOA) from isoprene oxidation as reported by

989   chamber studies in the literature and plotted as a function of the initial NO concentration and

990   relative humidity (RH). Yields are defined as the mass of SOA produced per unit mass of

991   isoprene oxidized. For studies with no detectable NO we plot the NO concentration as half the

992   reported instrument detection limit, and stagger points as needed for clarity. Data are colored by

993   relative humidity (RH). The thick grey line divides the low-NO_x and high-NO_x pathways as

994   determined by the fate of the $ISOPO_2$ radical (HO_2 dominant for the low-NO_x pathway, NO

995   dominant for the high-NO_x pathway). The transition between the two pathways occurs at a

996   higher NO concentration than in the atmosphere because HO_2 concentrations in the chambers are

997   usually much higher. Also shown as dashed line is the mean atmospheric yield of 3.3% for the

998   Southeast US determined in our study.

999
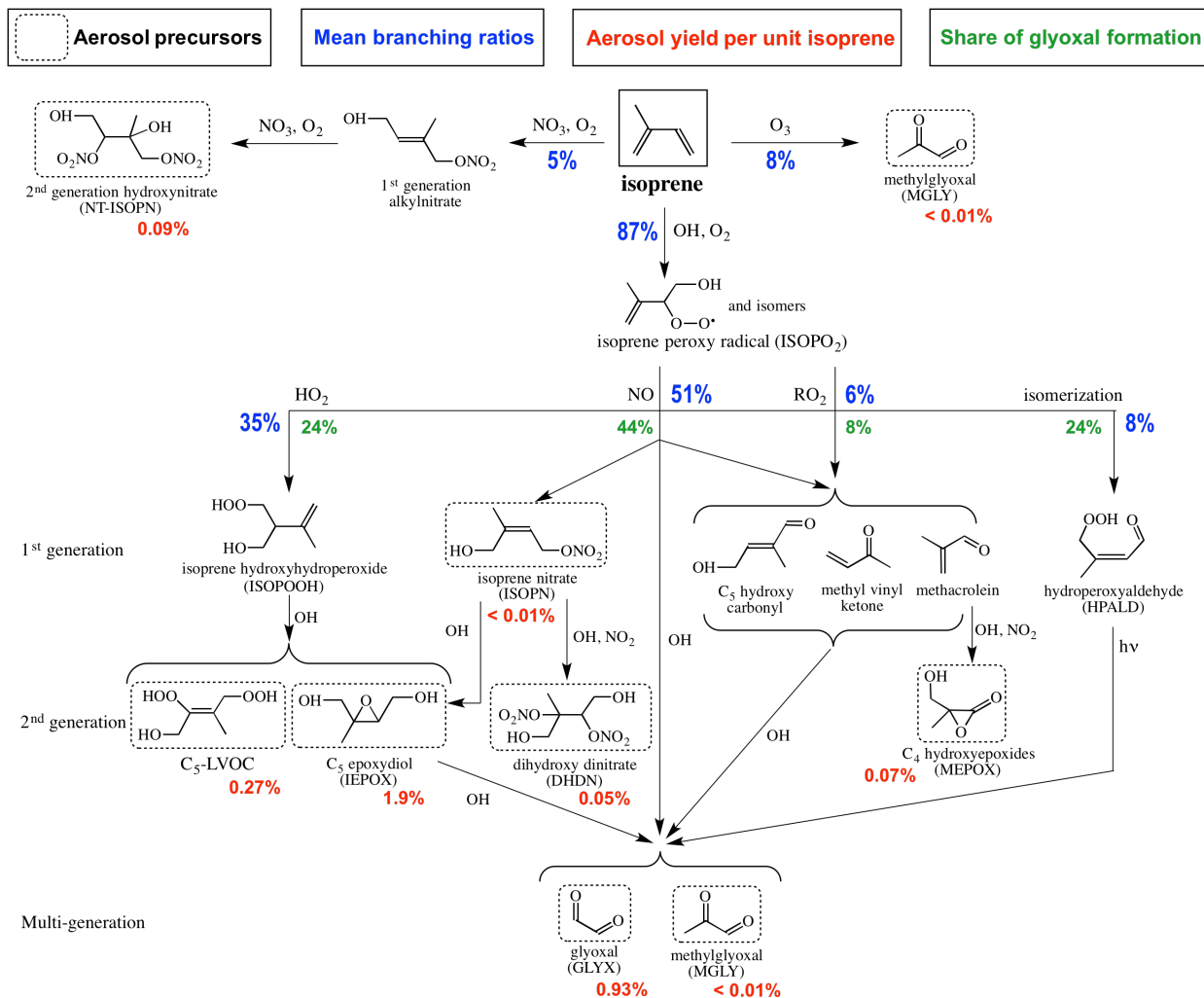
Figure 2. Gas-phase isoprene oxidation cascade in GEOS-Chem leading to secondary organic
aerosol (SOA) formation by irreversible aqueous-phase chemistry. Only selected species relevant
to SOA formation are shown. Immediate aerosol precursors are indicated by dashed boxes.
Branching ratios and SOA yields (aerosol mass produced per unit mass isoprene reacted) are
mean values from our GEOS-Chem simulation for the Southeast US boundary layer in summer.
The total SOA yield from isoprene oxidation is 3.3% and the values shown below the dashed
boxes indicate the contributions from the different immediate precursors adding up to 3.3%.
Contributions of high- and low-NO_x isoprene oxidation pathways to glyoxal are indicated.
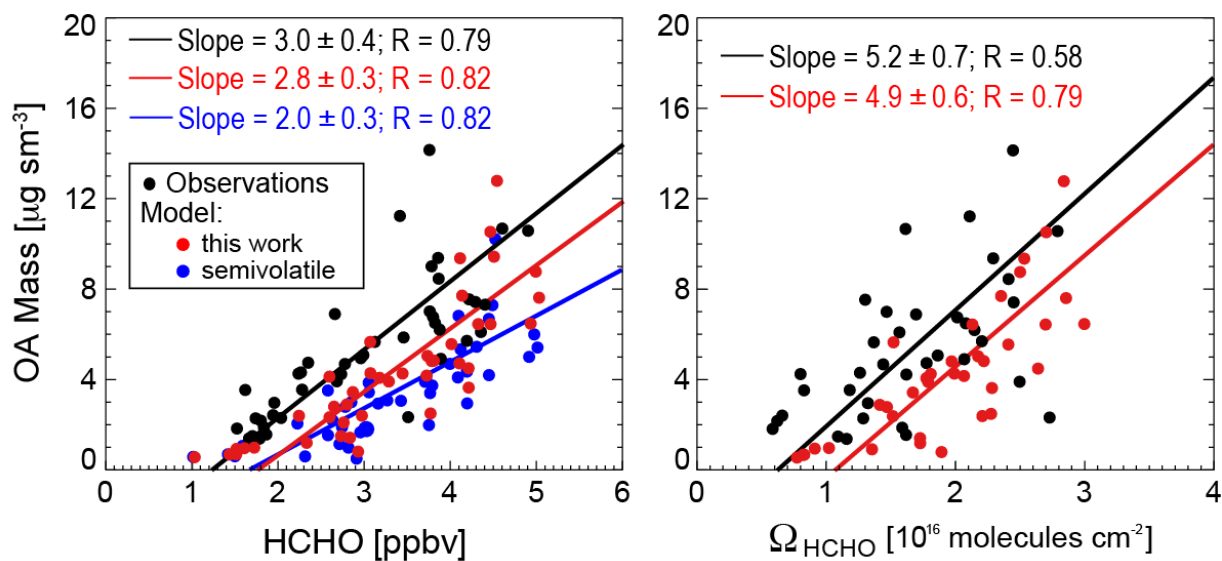
1008

Figure 3. Relationship of organic aerosol (OA) and formaldehyde (HCHO) concentrations over the Southeast US in summer. The figure shows scatterplots of SEAC[4]RS aircraft observations of OA concentrations in the boundary layer (< 2 km) vs. HCHO mixing ratios measured from the aircraft (left), and column HCHO (Ω_{HCHO}) retrieved from OMI satellite observations (right). Individual points are data from individual SEAC[4]RS flight days (August 8 - September 10), averaged on the GEOS-Chem grid. OMI data are for SEAC[4]RS flight days and coincident with the flight tracks. GEOS-Chem is sampled for the corresponding locations and times. Results from our simulation with aqueous-phase isoprene SOA chemistry are shown in red, and results from a simulation with the Pye et al. (2010) semivolatile reversible partitioning scheme are shown in blue. Aerosol concentrations are per m[3] at standard conditions of temperature and pressure (STP: 273 K; 1 atm), denoted sm[-3]. Reduced major axis (RMA) regressions are also shown with regression parameters and Pearson's correlation coefficients given inset. 1σ standard deviations on the regression slopes are obtained with jackknife resampling.
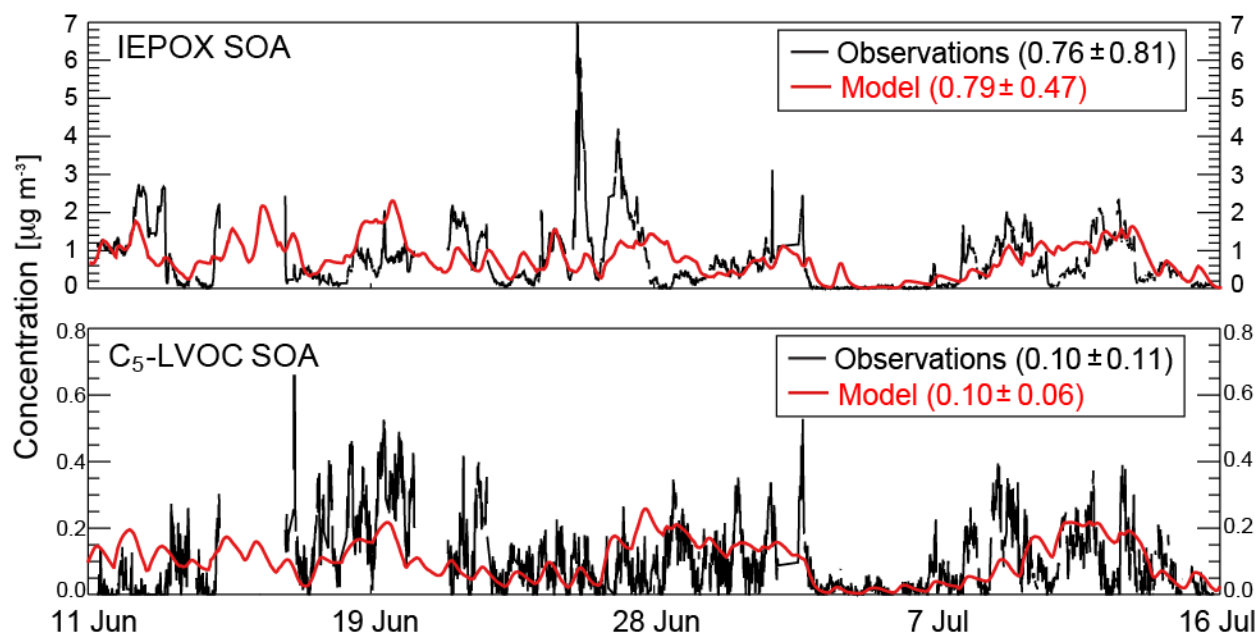
1022

1023

1024 **Figure 4.** Time series of the concentrations of isoprene SOA components at the SOAS site in

1025 Centreville, Alabama (32.94°N; 87.18°W) in June-July 2013: measured (black) and modeled

1026 (red) IEPOX SOA (top) and C_5-LVOC SOA (bottom) mass concentrations. Means and 1σ

1027 standard deviations are given for the observations and the model.
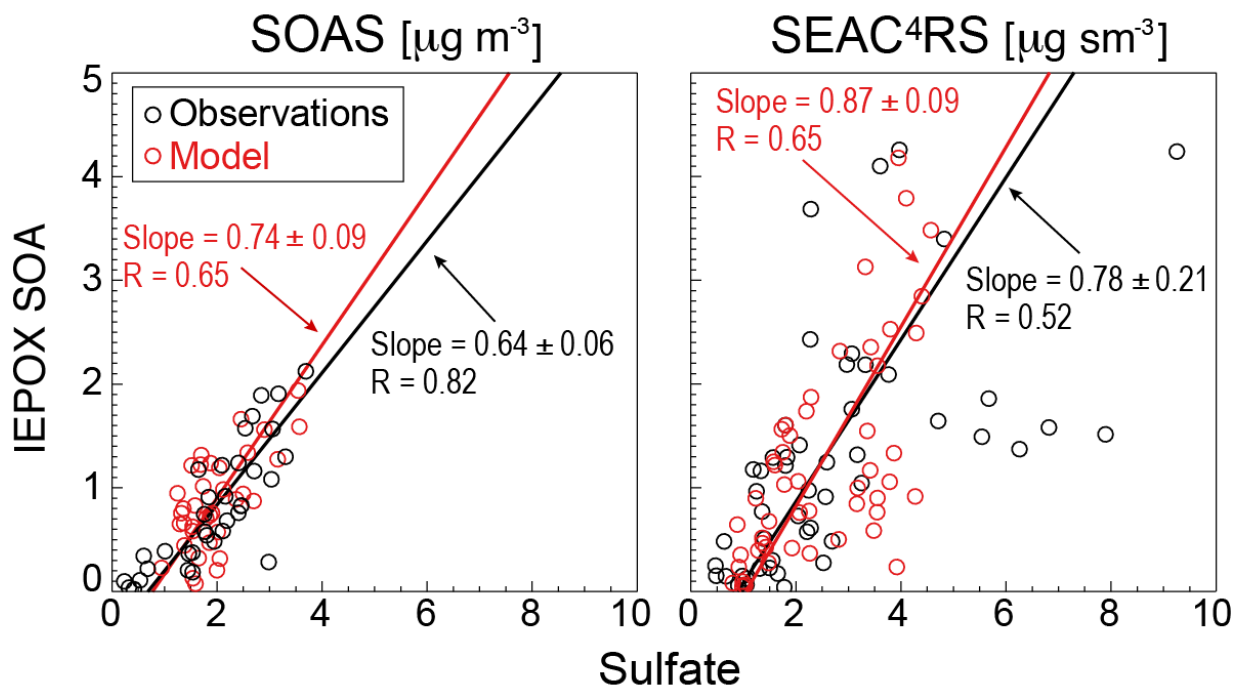
Figure 5. Relationship of IEPOX SOA and sulfate concentrations over the Southeast US in summer. Observed (black) and simulated (red) data are averages for each campaign day during SOAS (left), and boundary layer averages (< 2 km) for $2° \times 2.5°$ GEOS-Chem grid squares on individual flight days during SEAC[4]RS (right). RMA regression slopes and Pearson's correlation coefficients are shown. 1σ standard deviations on the regression slopes are obtained with jackknife resampling.

Boundary-layer IEPOX SOA and Sulfate Concentrations
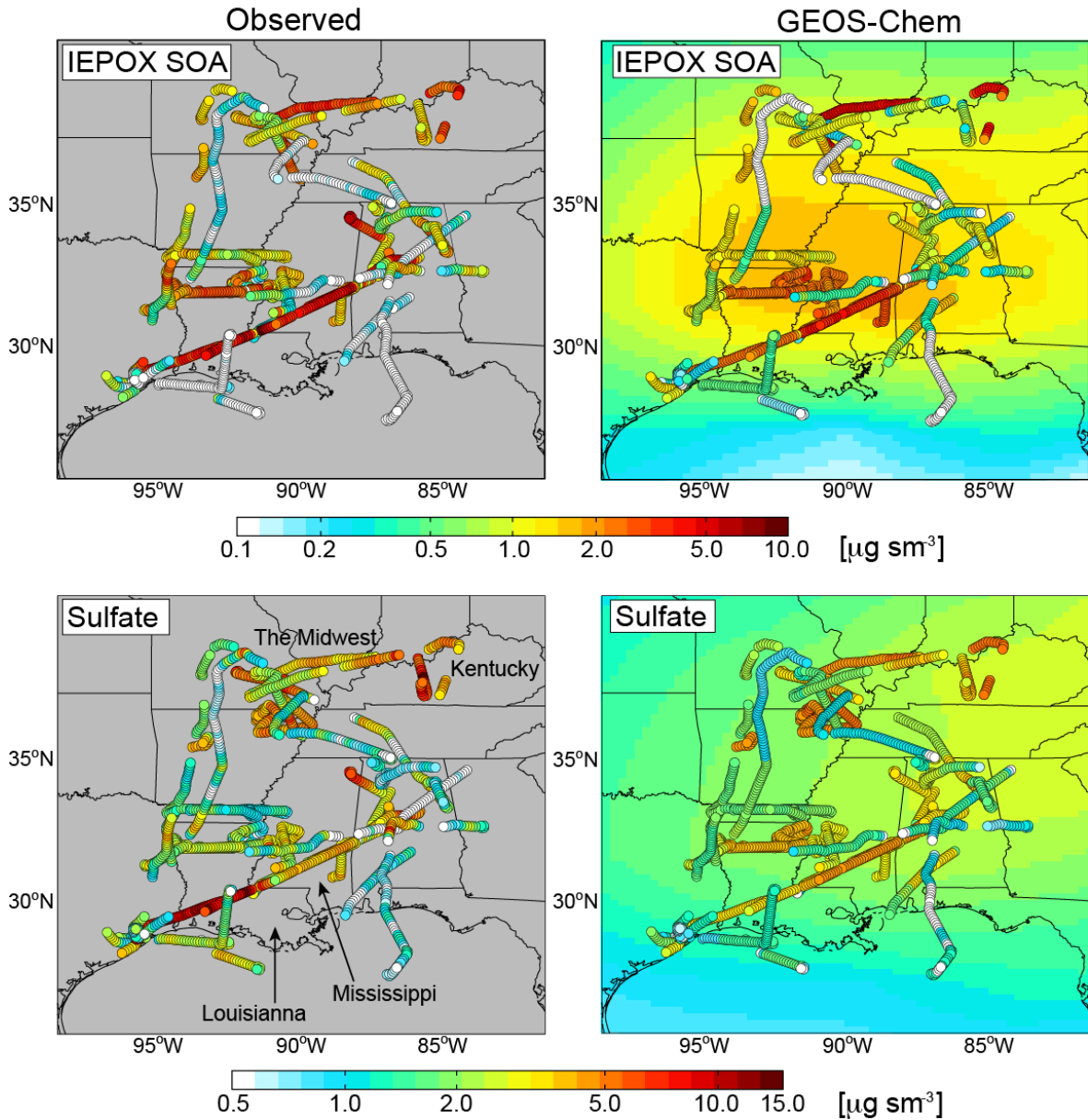
1035

1036 **Figure 6.** Spatial distributions of IEPOX SOA and sulfate concentrations in the boundary layer

1037 (<2 km) over the Southeast US during SEAC[4]RS (August-September 2013). Aircraft AMS

1038 observations of IEPOX SOA (top left) and sulfate (bottom left) are compared to model values

1039 sampled at the time and location of the aircraft observations (individual points) and averaged

1040 during the SEAC[4]RS period (background contours). Data are on a logarithmic scale.

1041
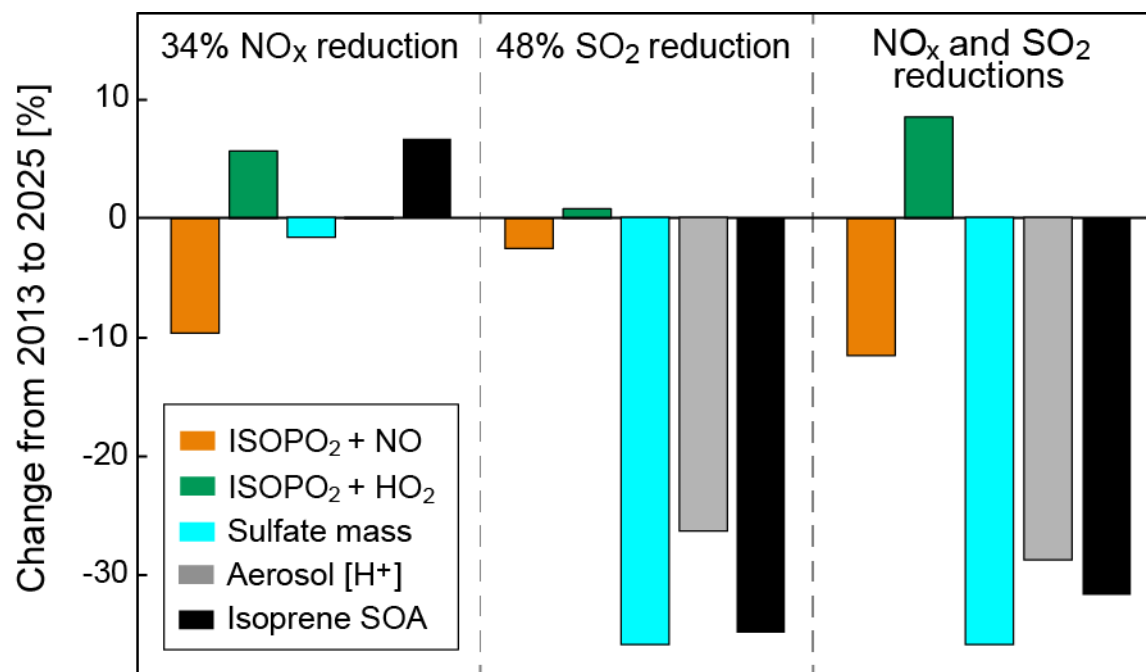
Figure 7. Effect of projected 2013-2025 reductions in US anthropogenic emissions on the formation of isoprene secondary organic aerosol (SOA). Emissions of NO_x and SO_2 are projected to decrease by 34% and 48%, respectively. Panels show the resulting percentage changes in the branching of $ISOPO_2$ between the NO and HO_2 oxidation channels, sulfate mass concentration, aerosol [H^+] concentration, and isoprene SOA mass concentration. Values are summer means for the Southeast US boundary layer.